Lithos 310–311 (2018) 1–19

Contents lists available at ScienceDirect

Lithos

journal homepage: www.elsevier.com/locate/lithos

Spinel and plagioclase peridotites of the Nain ophiolite (Central Iran): Evidence for the incipient stage of oceanic basin formation

Tahmineh Pirnia [a,*], Emilio Saccani [a], Shoji Arai [b]

[a] Department of Physics and Earth Sciences, Ferrara University, Ferrara 44122, Italy
[b] Department of Earth Sciences, Kanazawa University, Kanazawa 920-1192, Japan

ARTICLE INFO

Article history:
Received 7 December 2017
Accepted 1 April 2018
Available online 05 April 2018

Keywords:
Partial melting
Pargasite
Fertile spinel and plagioclase lherzolite
Subcontinental peridotite
Passive extension
Nain ophiolite
Central Iran

ABSTRACT

The Nain ophiolites crop out along the western border of the central East Iran Microcontinent (CEIM) and consist of an ophiolitic mélange in which pargasite-bearing spinel and plagioclase mantle lherzolites are largely represented. Whole-rock and mineral chemistry data suggest that these rocks record the complex history of the asthenospheric and lithospheric mantle evolution. The spinel lherzolites have experienced low-degree (~5%) partial melting and contain clinopyroxenes with positive Eu anomalies ($Eu/Eu^* = 1.10–1.48$) suggesting that the partial melting occurred under oxidized conditions (fayalite–magnetite–quartz −0.8 to +1.3). The pargasite and coexisting clinopyroxene in these rocks are depleted in light rare earth elements (LREE) (mean chondrite-normalized $Ce_N/Sm_N = 0.045$). The depleted chemistry of this amphibole reflects metasomatism during interaction with H_2O-rich subalkaline mafic melts, most likely concurrently with or after the partial melting of the spinel lherzolites. The plagioclase lherzolites were subsequently formed by the subsolidus recrystallization of spinel lherzolites under plagioclase facies conditions as a result of mantle uprising, as evidenced by: (1) the development of plagioclase rims around the spinels; (2) plagioclase + orthopyroxene exsolution textures within some clinopyroxene grains; (3) an increase in plagioclase modal content coupled with an increase in modal olivine and a decrease in modal pyroxene and pargasite; (4) coincident decreases in Al, Mg, and Ni, and increases in Cr, Ti, and Fe in spinel, as well as decreases in Al and Ca, and increases in Cr and Ti in pyroxene and pargasite; and (5) the identical whole rock compositions of the spinel and plagioclase lherzolites, which rules out a magmatic origin for the plagioclase in these units.

The Nain lherzolites have similar whole-rock and mineral geochemical compositions to subcontinental peridotites that are typically representative of Iberia-type rifted continental margins and ocean–continent transition zones (OCTZ), suggesting that they formed during the early stages of the evolution of the Nain oceanic basin. This means that the Nain lherzolites represent the Triassic–Jurassic western border of the CEIM or alternatively an associated OCTZ.

1. Introduction

Plagioclase peridotites form small portions by volume (~30%) of abyssal peridotites (Dick, 1989; Dick et al., 2010) and ophiolitic mantle sections, and also commonly occur in continental passive margin settings. Although they are commonly scattered and subordinate in volume, these peridotites are important geodynamic markers as they provide crucial information on the petrological and geodynamic processes associated with the evolution of the lithospheric mantle in extensional settings. These peridotites form as a result of two different petrological processes: (i) the impregnation of peridotites by basaltic melts (e.g., Dick, 1989) and (ii) the subsolidus recrystallization of peridotite under plagioclase facies conditions (e.g., Hamlyn and Bonatti, 1980). Melt-impregnated peridotites are formed by the porous migration, entrapment, and crystallization of basaltic melts within the hosting peridotites. This type of plagioclase peridotite generally forms in oceanic settings and are found in many ophiolitic complexes (e.g., Dick, 1989; Dick and Bullen, 1984; Dijkstra et al., 2001; Kaczmarek and Müntener, 2008; Müntener et al., 2004; Piccardo et al., 2004; Piccardo and Vissers, 2007; Pirnia et al., 2010; Rampone et al., 1997, 2008; Rampone and Borghini, 2008; Susini and Wezel, 1999; Tartarotti et al., 2002). The geochemistry of these melt-impregnated peridotites suggests they were depleted prior to melt impregnation (e.g., Kaczmarek and Müntener, 2008; Pirnia et al., 2010; Rampone et al., 1997, 2008; Susini and Wezel, 1999; Tartarotti et al., 2002). The residual chemistry of the hosting peridotites is interpreted to be the result of intense melting, which presumably records a mature stage of evolution of oceanic basins. Melt impregnation is usually preceded by melt–rock reactions (i.e., reactions between deeply sourced silica-undersaturated melts and peridotites) that cause pyroxene

* Corresponding author.
E-mail address: tahmineh.pirnia@gmail.com. (T. Pirnia).

https://doi.org/10.1016/j.lithos.2018.04.001

dissolution and the crystallization of olivine within the hosting peridotite (e.g., Dijkstra et al., 2001; Piccardo et al., 2004; Rampone et al., 2008).

In contrast, recrystallized plagioclase peridotites are formed by metamorphic reactions that take place when peridotites ascend from spinel- to plagioclase-facies conditions within the mantle. The general reaction for this transition is as follows: clinopyroxene (1) + orthopyroxene (1) + Al-spinel → clinopyroxene (2) + orthopyroxene (2) + Cr-spinel + olivine + plagioclase (e.g., Green and Hibberson, 1970; Kushiro and Yoder, 1966; Rampone et al., 1993). Recrystallized plagioclase peridotites are commonly found in Alpine-type peridotite massifs (Canil et al., 2003; Fabries et al., 1998; Furusho and Kanagawa, 1999; Green, 1964; Hoogerduijn Strating et al., 1993; Ozawa and Takahashi, 1995; Rampone et al., 1993, 1995, 2005) and ocean–continent transition zones (OCTZ; e.g., Hamlyn and Bonatti, 1980; Kornprobst and Tabit, 1988; Cannat and Seyler, 1995; Chazot et al., 2005; Montanini et al., 2006). This type of peridotite is indicative of cold tectonic exhumation of lithospheric mantle that is related to passive extension and thinning of lithosphere preceding ocean

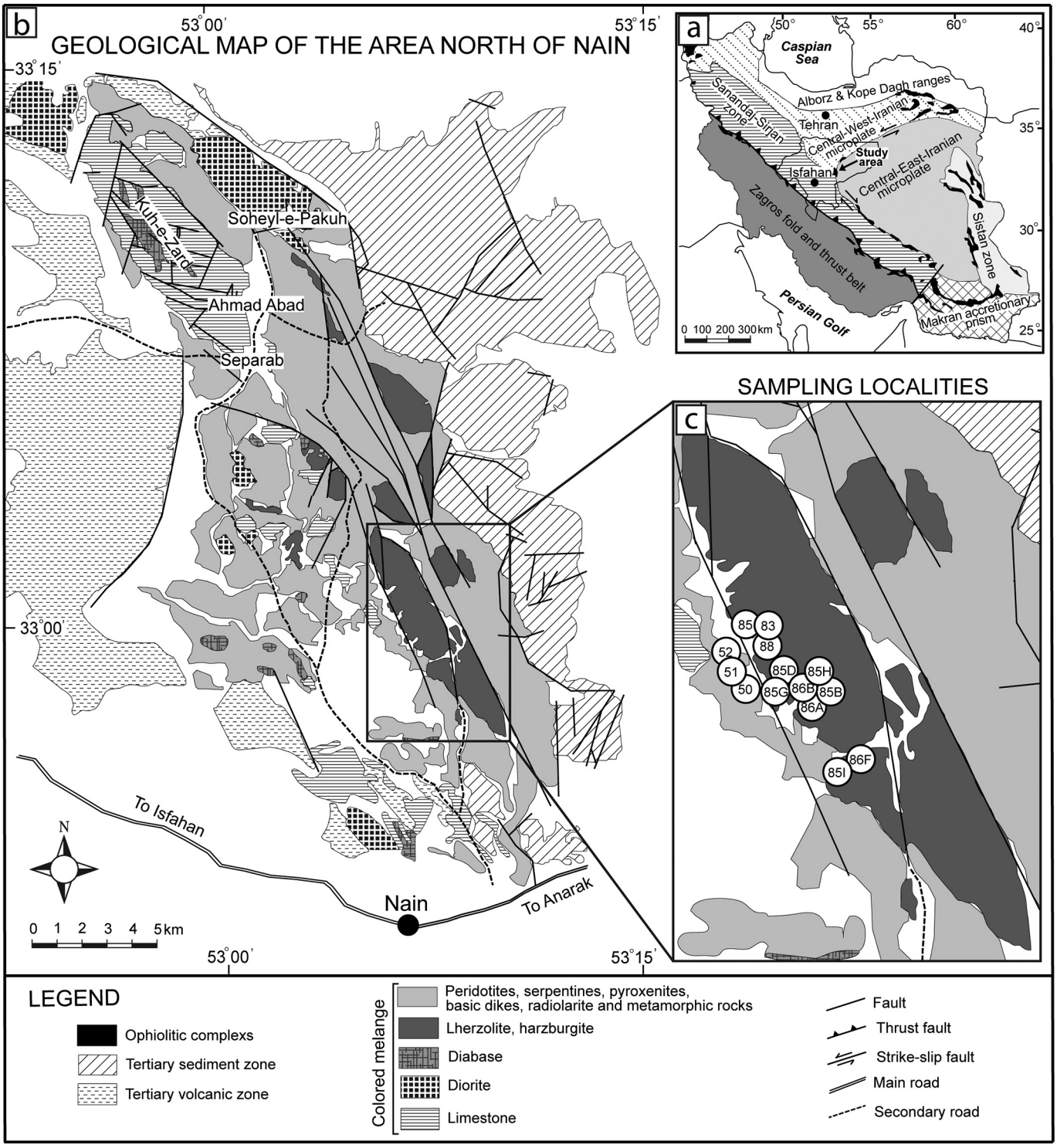

Fig. 1. (a) Simplified geological map of the area north of the town of Nain in Isfahan Province, central Iran (modified after Davoudzadeh, 1972). (b) Geological map of Iran. (c) Map of sample locations; note that the colored mélange unit is highly tectonized and contains ophiolitic material.

formation. Few studies have documented the processes of the spinel- to plagioclase-facies transition within mantle peridotites (e.g., Borghini et al., 2010, 2011; Chazot et al., 2005; Montanini et al., 2006; Rampone et al., 1993, 1995, 2005), and the majority of research on this topic has relied on laboratory experiments (e.g., Green and Falloon, 1998; Green and Ringwood, 1970; Presnall et al., 2002).

Iran is divided into the following main tectonic zones (Fig. 1a): (i) the Zagros fold-and-thrust belt, which is similar to the Arabian Plate; (ii) the Central–West Iran block, which represents the southern margin of Eurasia; (iii) the Central–East Iran microplate (CEIM), which is an independent microcontinental block; (iv) the Alborz and Kope Dag ranges, which contain rocks from the northern margin of the Iranian Plate that were folded during collision with Eurasia; (v) the Makran accretionary prism, which is the physiographic expression of a subduction zone along the southeastern coast of Iran. Iran contains numerous and widespread Mesozoic ophiolites that delineate suture zones between the different microcontinental blocks and plates (Fig. 1a). The Nain ophiolites crop out along the western border of the CEIM (Fig. 1a) and consist of an ophiolitic mélange dominated by tectonic slices of mantle peridotite. These mantle peridotites include relatively refractory clinopyroxene-bearing harzburgites as well as relatively fertile spinel and plagioclase lherzolites (e.g., Mehdipour Ghazi et al., 2010; Pirnia et al., 2010, 2013, 2014). The fertile spinel and plagioclase lherzolites are thought to record the transition from spinel- to plagioclase-facies mantle conditions, as also observed in the fertile lherzolites that characterize Iberia-type (or Alpine-type) continental margin ophiolites (Dilek and Furnes, 2011; Saccani et al., 2015). Several examples of continental margin ophiolites are found in the External Ligurian ophiolites in northern Italy (Rampone et al., 1995, 2005) and the Kizildag (Dilek et al., 1991) and Kermanshah (Saccani et al., 2013) ophiolites along the northern edge of the Arabian plate in SE Turkey–SW Iran. These types of continental margin ophiolites typically formed within the OCTZ as a consequence of amagmatic (or magma-starved) and asymmetric continental rifting (Robertson, 2007), which led to the exhumation of subcontinental lithospheric mantle.

This study presents new petrographic, mineral geochemical, and whole-rock geochemical data for fertile, pargasite-bearing spinel and plagioclase lherzolites from the Nain ophiolite. These data allow the identification of variations in mineral compositions and modes that are associated with the transition from spinel- to plagioclase-facies conditions in the upper mantle. The whole-rock geochemical data also enable the development of a new tectonic model of continental rifting and subsequent oceanic opening of the Mesozoic Neotethys sector to the west of the CEIM. These data demonstrate that continental rifting occurred after Iberia-type passive extension and provide new constraints on the reconstruction of the tectonic history of Iran.

2. Geological background

The Nain massif is considered part of the Nain–Baft ophiolitic belt, which consists of a series of ophiolitic massifs that crop out along the Nain–Dehshir and Dehshir–Baft strike-slip faults that delineate the southwestern boundary of the CEIM (e.g., Arvin and Robinson, 2011; Ghazi and Hassanipak, 2000; Shafaii Moghadam et al., 2010; Fig. 1a). These massifs consist of a series of tectonic slices that have been thrusted towards the southwest. The Nain ophiolite is located north of the town of Nain in Isfahan Province and crops out over an area of 480 km^2 with a NNW–SSE trend (Fig. 1b). This area contains ultramafic and mafic rocks along with radiolarites and limestones, all of which have been strongly intermingled by tectonic processes to form a "colored mélange" (Davoudzadeh, 1972; Pirnia et al., 2013; Fig. 1b). This tectonic disruption is dominated by numerous major and minor faults, the majority of which record vertical displacements. Peridotite masses have been extensively thrust up along these faults to form elongate oval-shaped bodies that are several kilometers long (Fig. 1b, c). The mantle rocks in the Nain ophiolite consist of clinopyroxene-bearing harzburgite spinel and plagioclase lherzolite lithologies, all of which are commonly serpentinized. Both harzburgites and serpentinites contain local dunite occurrences and chromitite pods (Mehdipour Ghazi et al., 2010; Pirnia et al., 2010, 2013, 2014). The mantle peridotites are locally cut by rodingite-altered or unaltered gabbro, pyroxenite, and wehrlite dikes. Similar to many harzburgites from the Mediterranean ophiolites (see Saccani et al., 2017 for a review), the Nain clinopyroxene-bearing harzburgites are thought to represent residual mantle formed in a subduction-related settings (e.g., Mehdipour Ghazi et al., 2010). The mantle plagioclase peridotites are commonly located proximal to shear zones and have fault-related textures that range from foliated to mylonitic (Pirnia et al., 2010, 2014). The mantle peridotites in the study area also contain small coarse-grained gabbro, isotropic gabbro, diorite, and gabbronorite plutons (Fig. 1b). The northern part of the Nain ophiolite contains small slices of volcanic rocks that consist of both pillowed and massive lavas. Rahmani et al. (2007) suggested that these volcanic rocks have tholeiitic to calc-alkaline affinities.

There is no general consensus on the tectonic setting of the Nain–Baft ophiolites, although two different models have been proposed: (i) they formed in a Cretaceous volcanic arc basin related to eastward subduction below the CEIM (e.g., Delaloye and Desmons, 1980; Desmons, 1982; Desmons and Beccaluva, 1983; Ghazi and Hassanipak, 2000); (ii) they are remnants of a Late Cretaceous backarc basin (e.g., Pirnia et al., 2010; Shafaii Moghadam et al., 2009; Shahabpour, 2005). Both of these models suggest that the Nain Basin was narrow and existed for ~45 Myr between the Cenomanian and the Paleocene (e.g., Davoudzadeh, 1972; Shafaii Moghadam et al., 2009).

3. Petrography

The Nain mantle peridotites can be texturally subdivided into: (i) porphyroclastic lherzolites that contain either spinel or spinel and plagioclase (Table 1), (ii) plagioclase-bearing mylonitic rocks. The following petrographic descriptions are given using the peridotite textural classification of Mercier and Nicolas (1975). Modal mineralogies for the peridotites were determined by point counting (2000 points per thin section). Further details of this modal analysis are provided in the footnote to Table 1.

Table 1
Modal compositions of representative examples of the Nain spinel and plagioclase lherzolites.

Texture	Rock type	Rock no.	Minerals					
			Ol%	Opx%	Cpx%	Spl%	Pl%	Amp%
Porphyroclastic	Spl-Lherzolite	83	63	23	8	3	–	3
		86-A	64	23	8	3	–	2
		86-B	63	24	7	3	–	3
	Pl-Lherzolite	85	65	22	7	3	1	2
		85-B	68	20	5	2	4	1
		85C	67	20	7	2	3	1
		85D	69	19	4	2	5	1
		85-E	65	21	6	3	3	2
		88	74	15	2	1	5	1
		85A	77	11	2	1	8	1
		85F	75	12	2	2	8	1
		85G	72	15	3	1	7	1
		85H	73	14	4	1	7	1
		85I	75	11	2	2	9	1
Mylonitic	Pl-Lherzolite	50	69	20	4	1.5	5	0.5
		52	74	14	4	1.5	6	0.5
		51	76	13	3.5	1	6	0.5

Footnote: modal compositions were calculated assuming that (a) mesh textured serpentine was originally olivine and (b) bastite compositions were originally orthopyroxene, and (c) discarding any late tensional veins filled with serpentine fibers, carbonate, or secondary minerals. Each modal analysis consisted of 2000 counts and lherzolites have clinopyroxene/pyroxene volume ratios of >0.1 (Arai, 1984). Abbreviations are as in Fig. 2.

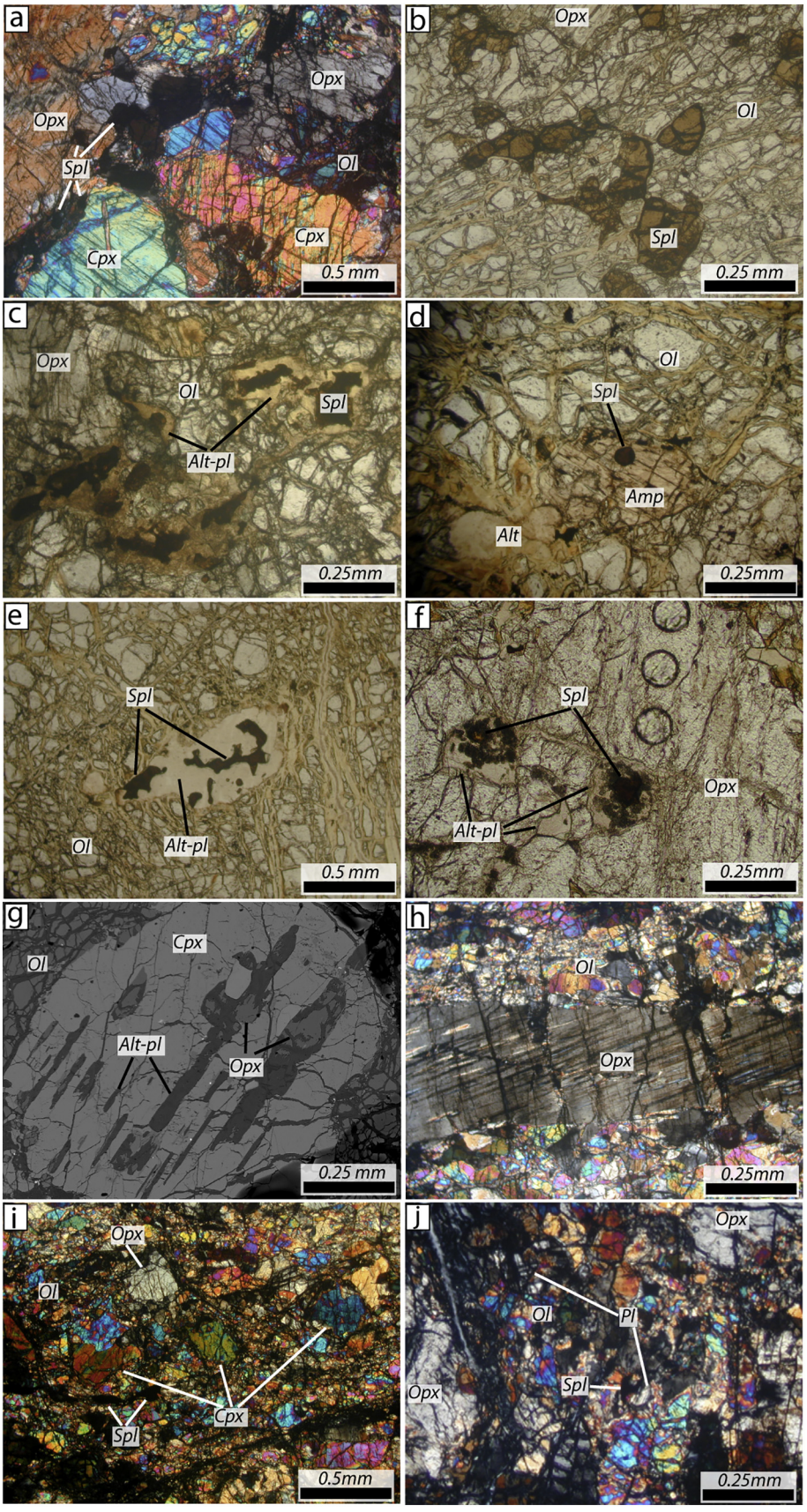
a
Opx
Opx
Spl
Ol
Cpx
Cpx
0.5 mm
b
Opx
Ol
Spl
0.25 mm
c
Opx
Ol
Spl
Alt-pl
0.25mm
d
Ol
Spl
Amp
Alt
0.25mm
e
Spl
Ol
Alt-pl
0.5 mm
f
Spl
Opx
Alt-pl
0.25mm
g
Cpx
Ol
Alt-pl
Opx
0.25 mm
h
Ol
Opx
0.25mm
i
Opx
Ol
Cpx
Spl
0.5mm
j
Opx
Ol
Pl
Spl
Opx
0.25mm

3.1. Porphyroclastic spinel and plagioclase peridotites

The porphyroclastic lherzolites range in texture from porphyroclastic spinel lherzolites to nearly granular plagioclase lherzolites (Fig. 2a, c, d). The spinel lherzolites are the most fertile samples within the studied peridotites and contain up to 8% modal clinopyroxene and 3% modal amphibole (Table 1). These lherzolites contain orthopyroxene and clinopyroxene porphyroclasts that usually include fine-grained globular spinel inclusions (Fig. 2a). Matrix-hosted spinels are light brown and subhedral to vermicular (Fig. 2b). The plagioclase lherzolites record the heterogeneous growth of plagioclase on spinel grains. Some portions of these rocks are entirely free of plagioclase and only contain subhedral light-brown spinel grains that are texturally similar to those occurring in spinel lherzolites. Conversely, other portions record the incipient formation of plagioclase in the form of thin plagioclase rims developed around spinel grains (Fig. 2c). The plagioclase within the porphyroclastic plagioclase lherzolites has been completely altered with the exception of one sample (88) in which they are partially preserved. Amphibole is distributed evenly within both spinel and plagioclase lherzolites, and occurs as isolated matrix-hosted crystals that locally have spinel cores (Fig. 2d) or as thin rims around orthopyroxene.

There is a clear positive correlation between the modal content of plagioclase and olivine, and a clear negative correlation between plagioclase and pyroxene contents within the plagioclase lherzolites (Table 1). The clinopyroxene porphyroclasts are rarely preserved but instead have generally been recrystallized to form smaller grains. The clinopyroxenes rarely contain exsolution lamellae consisting of an intergrown of plagioclase and orthopyroxene (Fig. 2g). When not enclosed in amphiboles, the spinel within plagioclase lherzolites containing high modal abundances of plagioclase is surrounded by thick plagioclase rims (Fig. 2e). In these plagioclase-rich lherzolites, pyroxenes show spinel inclusions partially recrystallized into plagioclase (Fig. 2f). The spinels within the plagioclase lherzolites are dark brown to black in color (Fig. 2e, f).

3.2. Mylonitic plagioclase peridotites

The mylonitic plagioclase peridotites are classified as mylonites using the fault-related rock classification of Sibson (1977). These rocks contain alternating porphyroclastic pyroxene-rich and recrystallized fine-grained layers consisting of olivine, orthopyroxene, clinopyroxene, plagioclase, spinel, and amphibole (Fig. 2h, i). The pyroxene-rich layers contain orthopyroxene porphyroclasts that are bent, are elongate parallel to the foliation plane (Fig. 2h), and are usually associated with thin amphibole overgrowths. In addition, amphiboles also occur as distinct small crystals within the recrystallized matrix. Clinopyroxene neoblasts are present within both layers, reach up to 1 mm in size (Fig. 2i), and do not have amphibole overgrowths. Spinels are present as either elongate porphyroclasts surrounded by plagioclase or as disseminated small crystals (with or without associated plagioclase) within the fine-grained matrix (Fig. 2j). The peridotite matrix contains plagioclase in contact with spinel as well as all other minerals. The plagioclase within the mylonite has also been altered but to a lesser extent than the plagioclase within the porphyroclastic lherzolites.

4. Analytical techniques

The major element compositions of minerals within 13 selected samples were determined using (1) a JEOL JXA8800R electron microprobe at Kanazawa University, Japan using an accelerating voltage of 20 kV and a probe current of 20 nA, and (2) a JEOL JXA8200 superprobe electron microprobe using an accelerating voltage of 15 kV and a probe current of 10 nA at Leoben University, Austria. The resulting data were corrected using an online ZAF program and are given in Supplementary Tables 1 to 6. Iron in silicate minerals is assumed to be Fe^{2+}, whereas Fe^{2+} and Fe^{3+} concentrations in spinels were determined using the approach of Droop (1987).

Orthopyroxene, clinopyroxene, and amphibole trace element abundances were determined by laser ablation–inductively coupled plasma–mass spectrometry (LA–ICP–MS) at two different laboratories: (1) Kanazawa University, Japan and (2) CNR-Istituto di Geoscienze e Georisorse, U.O.S. of Pavia, Italy. The measurements at Kanazawa University employed a MicroLas GeoLas Q-Plus LA system coupled to an ICP–MS system whereas the measurements at Pavia used a Quantel Brilliant 266 nm Nd:YAG laser source coupled to a Perkin Elmer DRC-e ICP–MS system. Laser spot diameters of 55 μm were used for the analysis of clinopyroxene and amphibole, whereas a laser spot diameter of 100 μm was used for orthopyroxene. All analyses used a laser frequency and energy of 10 Hz and 6 J/cm^2, respectively. External calibration used an NIST 612 standard at Kanazawa and an NIST 610 standard at Pavia. The accuracy of the data (reported in relative standard deviation (RSD%) terms) is better than 5% for the analyses at Kanazawa and better than 10% for the analyses at Pavia. Details of the analytical procedures used are given by Morishita et al. (2005a, 2005b) and Miller et al. (2012). The reproducibility between the two laboratories has been estimated to be better than 10% relative, based on the accuracy of the analyses of very similar standard materials. In addition, care was taken to ensure all spot analyses were located on crack-free and unaltered areas of the minerals being analyzed. In particular, the selection of analysis spots on pyroxenes avoided areas containing exsolution lamellae and plagioclase inclusions. The results of these trace element analyses are given in Supplementary Tables 7 to 9.

The whole-rock geochemical compositions of 11 selected samples were determined. Major and trace element compositions were determined using X-ray fluorescence (XRF) and pressed powder pellets employing an ARL Advant-XP automated X-ray spectrometer and the matrix correction methods outlined by Lachance and Trail (1966). Volatile contents were determined as loss on ignition (LOI) at 1000 °C. In addition, the concentrations of Rb, Sr, Zr, Y, Nb, Hf, Ta, Th, U, and the rare earth elements (REE) were determined by ICP–MS employing a Thermo Series X-I spectrometer. All whole-rock analyses are given in Supplementary Table 10. All major element compositions were recalculated on a LOI-free basis prior to plotting. The accuracy of XRF and ICP–MS analyses was evaluated using international standard rock samples run as unknowns. The detection limits for these analyses were also evaluated using the results of several analytical runs of a total of 29 international standards. XRF detection limits are <0.05 wt% and <3 ppm for major and trace elements, respectively, whereas ICP–MS detection limits range between 0.002 and 0.046 ppm. The XRF and ICP–MS data have accuracies of better than 8% and better than 10%, respectively. Full details of the accuracy and detection limits

Fig. 2. Photomicrographs of Nain spinel and plagioclase lherzolites, taken under plane polarized light barring (a), (h), (i), and (j), which were taken under cross-polarized light, and (g), which is a backscattered electron microprobe image. (a) Porphyroclasts of ortho- and clinopyroxene within a porphyroclastic spinel lherzolite. (b) Highly aluminous plagioclase-free spinel within the same sample as shown in (a). (c) Partly dissolved spinel within a porphyroclastic plagioclase lherzolite. (d) Pargasite containing spinel inclusions within a plagioclase harzburgite. (e) Highly dissolved spinel surrounded by a thick plagioclase rim within a plagioclase lherzolite. (f) Orthopyroxene spinel inclusions surrounded by thin overgrown plagioclase rims within a plagioclase lherzolite; circles show the locations of LA–ICP–MS analyses (Supplementary Table 7). (g) Backscattered electron microprobe image of a clinopyroxene porphyroclast containing exsolved orthopyroxene and plagioclase within a plagioclase lherzolite. (h) Elongate porphyroclast of orthopyroxene within a mylonitic lherzolite. (i) Fine-grained mylonite matrix containing neoblastic pyroxene. (j) Fine-grained plagioclase neoblasts within a fine-grained mylonitic matrix. Abbreviations are as follows: Ol, olivine; Opx, orthopyroxene; Cpx, clinopyroxene; Amp, amphibole; Spl, spinel; Pl, plagioclase; Alt, alteration products.

for all elements are given in Supplementary Table 11. All whole-rock analyses were undertaken at the Department of Physics and Earth Sciences, Ferrara University, Italy.

5. Mineral major-element compositions

5.1. Olivine

Olivine is forsteritic in composition. The forsterite contents [Fo = 100 × Mg/(Mg + Fe^{2+})] range from 89.1 to 90.2 within the porphyroclastic lherzolites, and from 89.9 to 91.0 within the mylonitic lherzolites (Fig. 3; Supplementary Table 1). The olivine is unzoned and in porphyroclastic lherzolites has Fo values that decrease slightly as plagioclase modal abundances increase (Table 1; Supplementary Table 1). The average Fo contents of these olivines decrease from 90.0 in the spinel lherzolite to 89.5 in the plagioclase lherzolite (which contains up to 9% modal plagioclase; Table 1). These olivines contain 0.26–0.42 wt% NiO and show compositional variations that all lie within the range of compositions of mantle olivine (Takahashi et al., 1987).

5.2. Spinel

All of the spinels with plagioclase rims within the porphyroclastic peridotites are chemically zoned, with decreases in Al and increases in Ti, Cr, and Fe from core to rim (Figs. 4 and 5; Supplementary Table 2). This chemical zonation is more intense in spinels within lherzolites containing higher modal abundances of plagioclase (Table 1; Supplementary Table 2). Although strongly zoned, the spinel cores within the plagioclase lherzolites are compositionally comparable to those within the spinel lherzolites (Figs. 4 and 5; Supplementary Table 2). The spinels with the lowest Cr# [Cr# = Cr/(Cr + Al)] values (0.10) occur as isolated grains within the spinel lherzolites (Supplementary Table 2). On average, spinels within plagioclase lherzolites have much higher Cr# values (0.26) than the spinel within spinel lherzolites (0.15; Figs. 4 and 5; Supplementary Table 2). The spinels within mylonites have moderately high Cr# values (0.28–0.34) and TiO_2 contents (0.11–0.28 wt%; Fig. 5; Supplementary Table 2).

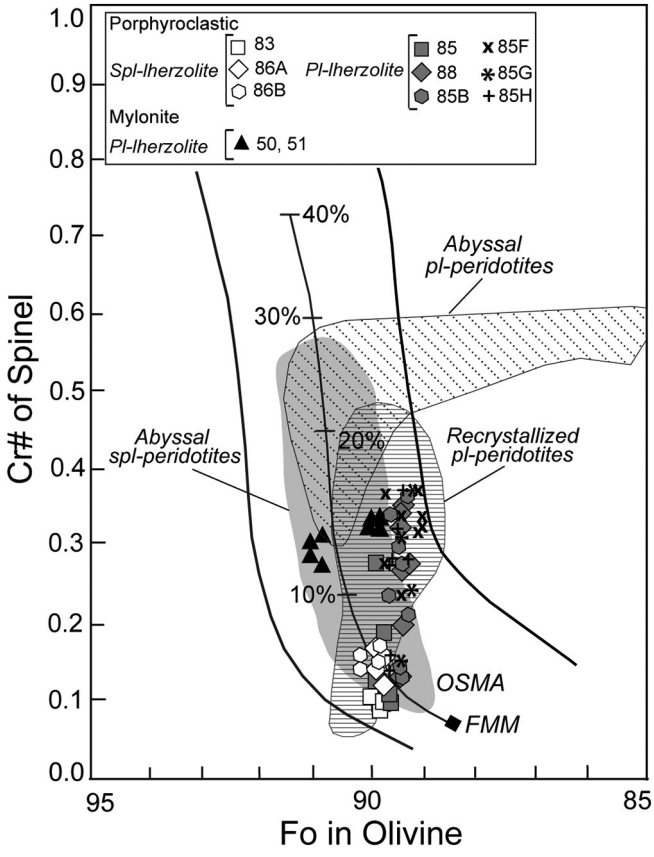

Fig. 3. Spinel Cr# versus olivine Fo diagram for spinel and plagioclase lherzolites of the Nain ophiolite. The compositional range of mantle peridotites (ol–spl mantle array, OSMA), the melting curve, and the abyssal spinel peridotite compositions are from Arai (1994). FMM denotes the fertile MOR (mid-ocean ridge) mantle. The diagram also shows fields representing the range of compositions of abyssal plagioclase peridotites (Constantin, 1999; Dick, 1989; Dick et al., 2010; Ohara et al., 2002; Seyler and Bonatti, 1997; Susini and Wezel, 1999; Tartarotti et al., 2002) and recrystallized plagioclase peridotites (Chazot et al., 2005; Montanini et al., 2006; Rampone et al., 1993, 1995, 2005).

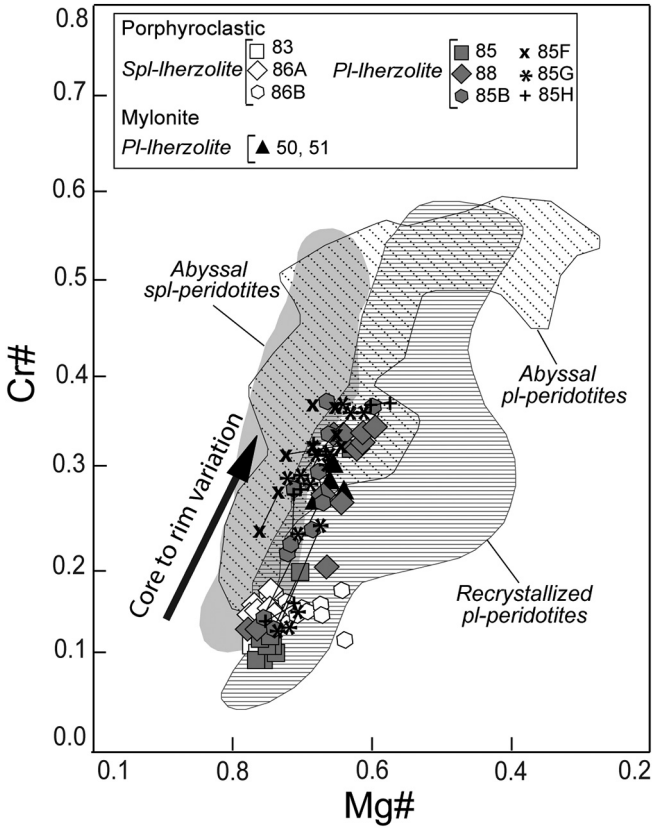

Fig. 4. Spinel Cr# versus Mg# diagram for spinel and plagioclase lherzolites of the Nain ophiolite along with fields for abyssal spinel peridotites (Dick and Bullen, 1984), abyssal plagioclase peridotites (Dick, 1989; Dick et al., 2010; Dick and Bullen, 1984; Loocke and Snow, 2013; Ohara et al., 2002; Seyler and Bonatti, 1997; Susini and Wezel, 1999; Tartarotti et al., 2002), and recrystallized plagioclase peridotites (Cannat and Seyler, 1995; Chazot et al., 2005; Hoogerduijn Strating et al., 1993; Kornprobst and Tabit, 1988; Montanini et al., 2006; Rampone et al., 1993, 1995, 2005). Solid lines connect core and rim compositions, and arrows indicate chemical variations from core to rim.

5.3. Orthopyroxene

Orthopyroxenes are enstatitic in compositions and show consistent Mg# [Mg# = (Mg/(Mg + Fe^{2+})] values within the porphyroclastic peridotites (0.905) but variable Mg# values within the mylonites (0.898–0.911; Fig. 6a; Supplementary Table 3). The orthopyroxenes are chemically zoned in the porphyroclastic lherzolites with Al_2O_3 contents that decrease from core (mean of 4.26 wt%) to rim (mean of 3.50 wt%; Fig. 6c, e; Supplementary Table 3). This decrease in Al_2O_3 contents is associated with a decrease in Cr_2O_3 within the spinel lherzolites and an increase in Cr_2O_3 within the plagioclase lherzolites (Supplementary Table 3). The orthopyroxenes within the plagioclase lherzolites contain higher mean concentrations of Cr_2O_3 (0.47 wt%) than the orthopyroxenes within the spinel lherzolites (0.42 wt%; Fig. 6a; Supplementary Table 3). A similar decrease in orthopyroxene

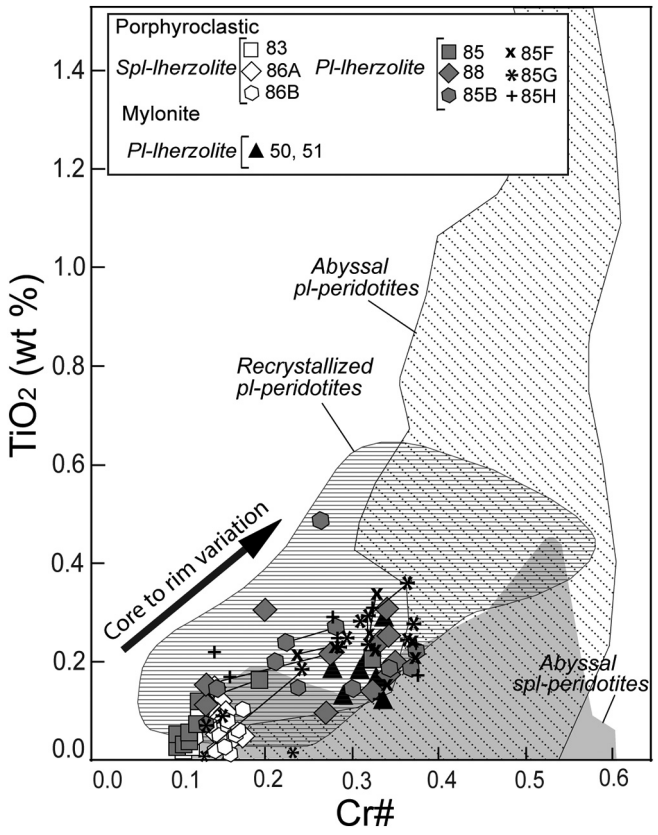

Fig. 5. Spinel TiO_2 versus Cr# diagram for spinel and plagioclase lherzolites of the Nain ophiolite along with fields for abyssal spinel peridotites (Dick and Bullen, 1984; Seyler and Bonatti, 1997), abyssal plagioclase peridotites (Cannat et al., 1997; Dick, 1989; Dick et al., 2010; Dick and Bullen, 1984; Loocke and Snow, 2013; Ohara et al., 2002; Seyler and Bonatti, 1997; Susini and Wezel, 1999; Tartarotti et al., 2002), and recrystallized plagioclase peridotites (Cannat and Seyler, 1995; Chazot et al., 2005; Hoogerduijn Strating et al., 1993; Kornprobst and Tabit, 1988; Montanini et al., 2006; Rampone et al., 1993, 1995, 2005). Solid lines connect core and rim compositions, and arrows indicate chemical variations from core to rim.

Al_2O_3 content from core to rim is also present within the mylonites (Supplementary Table 3), although this decrease is not systematically associated with any increase in Cr_2O_3 content. Orthopyroxene cores adjacent to plagioclase inclusions contain relatively low concentrations of Al_2O_3 and Cr_2O_3, similar to the rims of these orthopyroxenes (Supplementary Table 3).

5.4. Clinopyroxene

Clinopyroxenes are mostly diopsidic in composition and yield a mean CaO concentration of 22.9 wt% (Supplementary Table 4). All of these clinopyroxenes are chemically zoned and have $A1_2O_3$ concentrations that decrease from core to rim (Fig. 6d, f; Supplementary Table 4), independent from variations in Cr_2O_3 content. Although with different behavior in different rocks, the TiO_2 and Na_2O contents generally show mutual correlation (Supplementary Table 4). In spinel lherzolites, their contents decrease from cores to rims, whereas in plagioclase lherzolites their contents increase from core to rim (Fig. 6d; Supplementary Table 4). The clinopyroxenes within mylonites have lower mean Al_2O_3 contents (2.44–5.31 wt%) but higher mean Cr_2O_3 contents (0.64–1.16 wt%) than the clinopyroxenes within the porphyroclastic lherzolites (Al_2O_3 = 2.87–6.35 wt%; Cr_2O_3 = 0.53–1.07 wt%; Fig. 6b, d; Supplementary Table 4).

5.5. Amphibole

The amphiboles show pargasite compositions based on the classification of Leake et al. (1997). All of these amphiboles have compositions very close to the ideal pargasite formula, with low K_2O contents (<0.04 wt%; Supplementary Table 5). Their TiO_2 contents range from 1.09 to 3.35 wt% and their Mg# ranges from 0.877 to 0.921 (Fig. 7a; Supplementary Table 5). Amphiboles within the mylonites have uniform compositions (Fig. 7a–f; Supplementary Table 5) whereas the amphiboles within the porphyroclastic samples vary in composition between the spinel and plagioclase lherzolites (Fig. 7a–f; Supplementary Table 5). In particular, the amphiboles within the plagioclase lherzolites contain lower concentrations of Al_2O_3 (mean of 13.9 wt%) but higher concentrations of Ti_2O (mean of 1.92 wt%) than the amphiboles within the spinel lherzolites (mean Al_2O_3 of 14.6 wt% and mean Ti_2O of 1.22 wt%; Fig. 7a, b).

5.6. Plagioclase

The plagioclase relics within porphyroclastic lherzolite sample 88 have a bytownite composition (mean of An_{81}) and are free of orthoclase components (Supplementary Table 6). The plagioclase within the mylonites also has a bytownite composition but with a wider range of compositional variations (An_{71}–An_{87}) that are associated with the mylonitization process. These anorthite contents are independent on the mineral occurrence or texture.

6. Trace element mineral chemistry

6.1. Orthopyroxene

The orthopyroxenes contain very low REE concentrations (<4 times the chondrite composition of Sun and McDonough, 1989) and have strongly fractionated REE patterns with a mean Chondrite-normalized (Sun and McDonough, 1989) Ce_N/Yb_N value of 0.008 (Fig. 8a, c, e; Supplementary Table 7). These REE compositions are expected for orthopyroxenes within mantle peridotites. The orthopyroxenes within the plagioclase lherzolites have higher heavy REE (HREE) and lower middle (MREE) to light REE (LREE) concentrations than those in the spinel lherzolites (Fig. 8a, c; Supplementary Table 7). The multi-element variation diagram patterns for these orthopyroxenes show positive Ti anomalies (Fig. 8b, d, f). In addition, the orthopyroxenes within the spinel lherzolites have slight to significantly elevated positive Eu anomalies (Eu/Eu^* = 1.01–1.69; Fig. 8a, b; Supplementary Table 7).

6.2. Clinopyroxene

The clinopyroxenes have fractionated REE patterns that are depleted in the LREE and have flat MREE to HREE patterns at ~5 to 11 times chondrite abundances (Sun and McDonough, 1989; Fig. 9a, c, e). The clinopyroxenes within the porphyroclastic plagioclase lherzolites have either positive or negative Eu anomalies (Eu/Eu^* = 0.69–1.16; Fig. 9d, f; Supplementary Table 8), where the positive Eu anomalies show a negative correlation with plagioclase modal abundances (Table 1). In contrast, the clinopyroxenes within the spinel lherzolites have positive Eu anomalies (Eu/Eu^* = 1.10–1.48; Fig. 9b). The clinopyroxenes within the plagioclase lherzolites are slightly enriched in the REE and trace elements, barring Eu and Sr, relative to those within the spinel lherzolites (Fig. 9a–d; Supplementary Table 8). The clinopyroxenes within the mylonites have slightly negative to negative Eu anomalies (Eu/Eu^* = 0.73–0.95).

6.3. Amphibole

Amphiboles have similar REE patterns to coexisting clinopyroxenes in that they are LREE depleted (mean Ce_N/Sm_N = 0.045) with almost

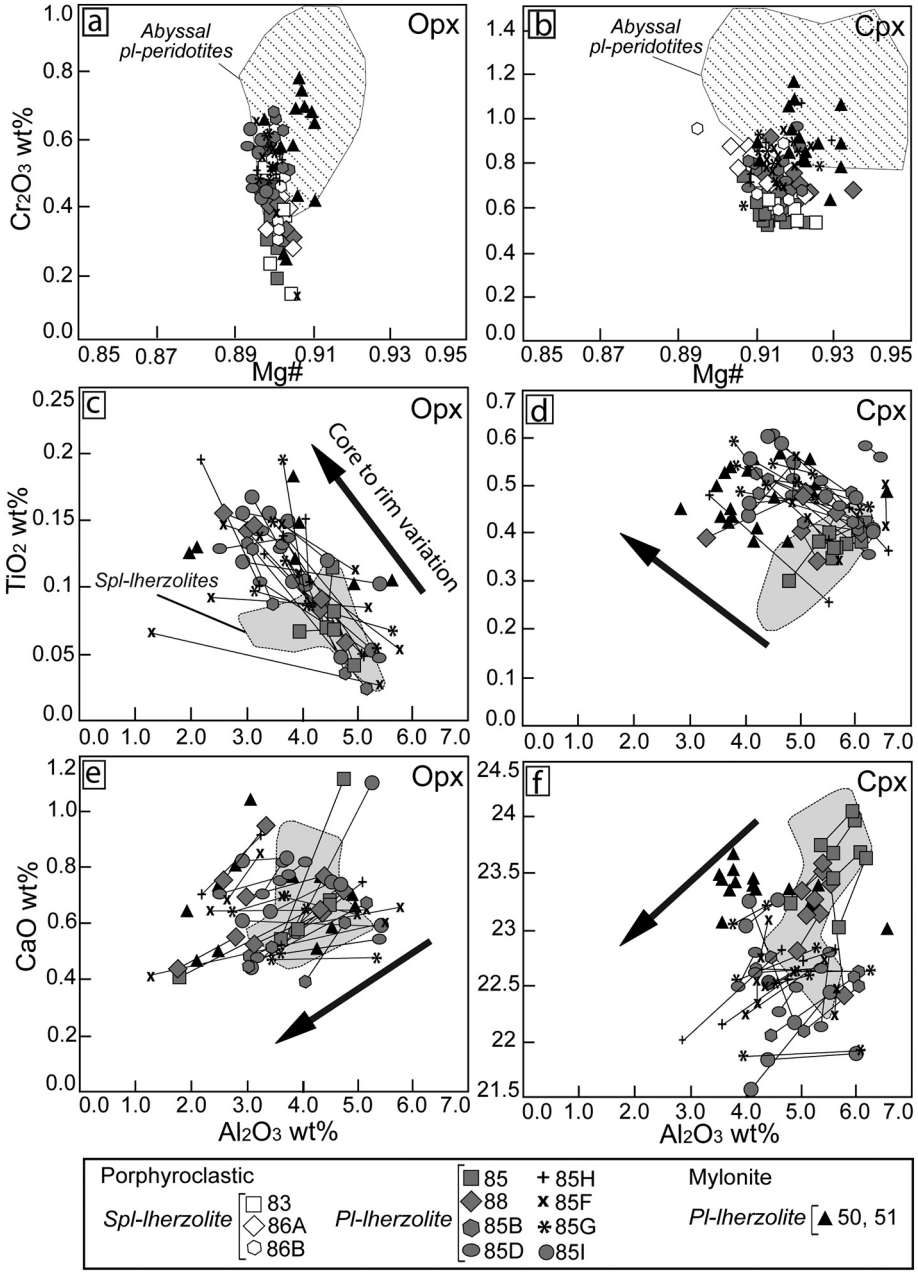

Fig. 6. Variations in orthopyroxene (a, c, and e) and clinopyroxene (b, d, and f) compositions within spinel and plagioclase lherzolites from the Nain ophiolite. (a) and (b) show variations in Cr_2O_3 concentrations versus Mg# values, (c) and (d) show variations in TiO_2 versus Al_2O_3 contents, and (e) and (f) show variations in CaO versus Al_2O_3 contents. (a) and (b) also show the range in compositions of pyroxenes within abyssal plagioclase peridotites (Dick, 1989; Dick et al., 2010; Tartarotti et al., 2002). Solid lines connect core and rim compositions, and arrows indicate chemical variations from core to rim.

flat MREE to HREE patterns (mean $Gd_N/Yb_N = 0.90$) at ~10–13 times chondrite abundance (Sun and McDonough, 1989; Fig. 10a–c; Supplementary Table 9). The amphiboles within the porphyroclastic plagioclase lherzolites are also similar to the pyroxenes in that they contain slightly higher REE and trace element concentrations than the amphiboles within the spinel lherzolites (Fig. 10a, b; Supplementary Table 9). Similar to pyroxenes, amphiboles within the spinel lherzolites also have positive Eu anomalies ($Eu/Eu^* = 1.03–1.14$; Fig. 10a; Supplementary Table 9).

7. Whole-rock major and trace element geochemistry

The effect of alteration on the mobility of major and trace elements in the samples was determined by plotting major elements against MgO and LOI values (not shown). The lack of any correlation between SiO_2, Al_2O_3, FeO, MgO, CaO, Na_2O, and Ni concentrations with LOI values (e.g., r^2 LOI–$SiO_2 = 0.23$; r^2 LOI–$Al_2O_3 = 0.03$; r^2 LOI–FeO = 0.08; r^2 LOI–MgO = 0.17; r^2 LOI–CaO = 0.20; r^2 LOI–$Na_2O = 0.03$; r^2 LOI–Ni = 0.03) suggests that these elements were not significantly mobilized during alteration of the peridotites. In addition, the concentration of a number of elements correlate well with MgO concentrations (e.g., r^2 MgO–$SiO_2 = 0.72$; r^2 MgO–$Al_2O_3 = 0.81$; r^2 MgO–FeO = 0.77; r^2 MgO–CaO = 0.77; r^2 MgO–$Na_2O = 0.91$; r^2 MgO–Ni = 0.72), again suggesting that these elements have not been significantly mobilized. In addition, all of the samples plot close to the "terrestrial array" for fresh mantle peridotites on a MgO/SiO_2 vs. Al_2O_3/SiO_2 diagram (not shown; Jagoutz et al., 1979), indicating that these mantle peridotites have undergone limited (if any) mobilization of SiO_2, Al_2O_3, and MgO contents.

The concentrations of Al_2O_3, CaO, and V (Fig. 11a, b; Supplementary Table 10), as well as SiO_2 and Na_2O, in both spinel and plagioclase

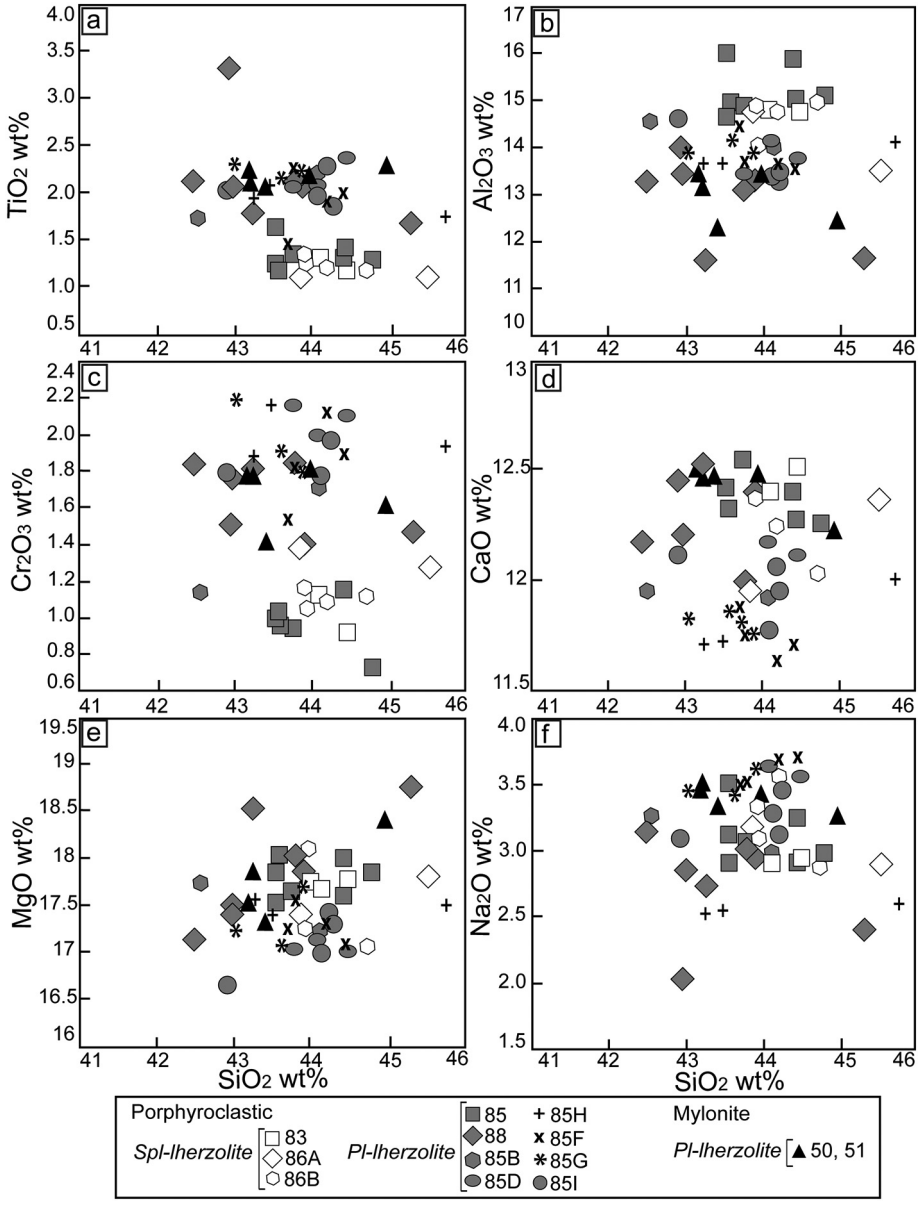

Fig. 7. Diagrams showing variations in (a) TiO_2, (b) Al_2O_3, (c) Cr_2O_3, (d) CaO, (e) MgO, and (f) Na_2O contents versus SiO_2 within pargasite in spinel and plagioclase lherzolites of the Nain ophiolite.

lherzolites negatively correlate with MgO concentrations. In contrast, Ni, FeO, and Co concentrations positively correlate with MgO (Supplementary Table 10). Both plagioclase and spinel lherzolites have similar whole-rock geochemical compositions (Supplementary Table 10) that are characterized by low concentrations of TiO_2 (0.05–0.08 wt%) and high concentrations of Ni (1806–1919 ppm) and Cr (2259–2699 ppm). They also contain relatively high concentrations of Al_2O_3 (2.75–3.86 wt%), CaO (1.92–2.97 wt%), Zr (1.22–2.79 ppm), and Y (1.51–3.35 ppm), all of which are typical for slightly depleted peridotites. Both spinel (Mg# = 0.901–0.903) and plagioclase (Mg# = 0.895–0.898) lherzolites also have similar Mg# values. In general, these rocks have whole-rock major and trace element compositions that are similar to those of the subcontinental mantle peridotites that crop out within the External Ligurian ophiolitic units of the northern Apennines (Ottonello et al., 1984; Rampone et al., 1993, 1995; Fig. 11).

All of the lherzolites contain relatively high concentrations of the HREE (e.g., Yb_N = 0.99–2.06; Fig. 12a, b). However, the plagioclase lherzolites are depleted in the LREE with respect to both the MREE and HREE (Ce_N/Sm_N = 0.09–0.22; Ce_N/Yb_N = 0.04–0.11). They have chondrite-normalized REE patterns (Fig. 12b) that are similar to those of subcontinental mantle peridotites within the Erro–Tobbio peridotites of the Ligurian Alps, Italy (Rampone et al., 2005). In contrast, the spinel lherzolites have lower LREE/MREE (Ce_N/Sm_N = 0.39–0.46) and LREE/MREE (Ce_N/Yb_N = 0.18–0.19) values, and chondrite-normalized REE patterns that partially overlap those of the subcontinental peridotites of the External Ligurian and Erro–Tobbio ophiolites (Ottonello et al., 1984; Rampone et al., 1993, 1995, 2005). In general, both plagioclase and spinel lherzolites are relatively enriched in the REE (Fig. 12), indicating that both these rocks represent slightly depleted mantle peridotites. This inference is consistent with their high Al_2O_3/SiO_2 ratios (0.065–0.089), which are much higher than those of peridotites that represent the residual mantle after mid-ocean ridge basalt (MORB)-type melt extraction in mid-ocean ridge settings (Al_2O_3/SiO_2 = 0.030–0.060; Saccani et al., 2013).

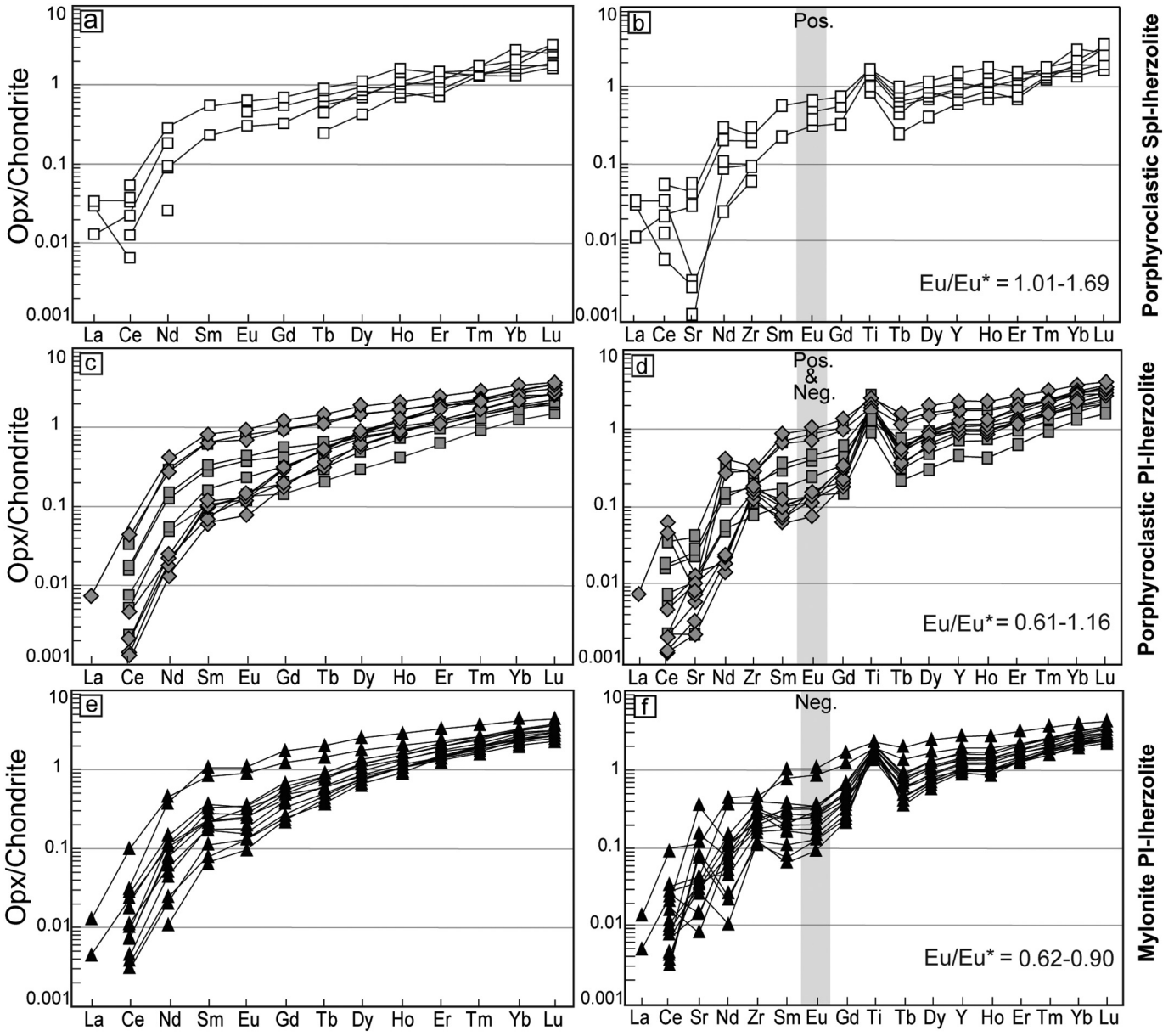

Fig. 8. Chondrite-normalized (a, c, and e) REE and (b, d, and f) multi-element variation diagram patterns for orthopyroxenes from the Nain spinel and plagioclase lherzolites normalized to the chondrite composition of Sun and McDonough (1989). Orthopyroxenes from porphyroclastic spinel lherzolites are shown in (a) and (b), from porphyroclastic plagioclase lherzolites are shown in (c) and (d), and from mylonite plagioclase lherzolites are shown in (e) and (f). Grey columns highlight Eu values, and positive and negative anomalies are denoted by Pos. and Neg., respectively.

8. Thermobarometry

Temperature estimates were undertaken using the thermometers of Brey and Köhler (1990), Witt-Eickschen and Seck (1991), and Liang et al. (2013). The two-pyroxene thermometer of Brey and Köhler (1990) is based on the exchange of orthopyroxene components between coexisting pyroxenes, whereas the orthopyroxene thermometers of Brey and Köhler (1990) and Witt-Eickschen and Seck (1991) are based on the solubility of Al and Ca in orthopyroxene. The thermometer of Liang et al. (2013) is based on the partitioning of the REE between coexisting clinopyroxenes and orthopyroxenes, and is used to estimate the closure temperature of the peridotites, whereas the thermometers of Brey and Köhler (1990) and Witt-Eickschen and Seck (1991) yield estimates of cooling temperatures. Temperature estimates were based on pyroxene core compositions and are given in Table 2. The Brey and Köhler (1990) and Witt-Eickschen and Seck (1991) thermometers yield similar ranges of equilibration temperatures for the porphyroclastic spinel (834 °C–939 °C) and plagioclase (823 °C–941 °C) lherzolites. The mylonites have a more limited and slightly lower temperature range (877 °C–899 °C) than the porphyroclastic lherzolites. However, it should be noted that the tectonic disruption (e.g., fine grain-size) experienced by these rocks may have affected these temperature estimates. There are no correlations between modal plagioclase contents and temperature estimates. The temperatures estimated using the Liang et al. (2013) method (991 °C–1101 °C) are about 150 °C higher than the temperatures obtained using the other methods. This difference is similar to that observed in Alpine subcontinental peridotites, but is much lower than the differences observed in abyssal peridotites (Dygert and Liang, 2015).

The barometer of Nimis and Ulmer (1998) is the only method that can be used to estimate equilibration pressures for all of the samples in the study area because it is based on clinopyroxene compositions. On average, spinel lherzolites yield equilibration pressures of ~0.60 GPa (Table 2), whereas the plagioclase lherzolites yield lower pressures

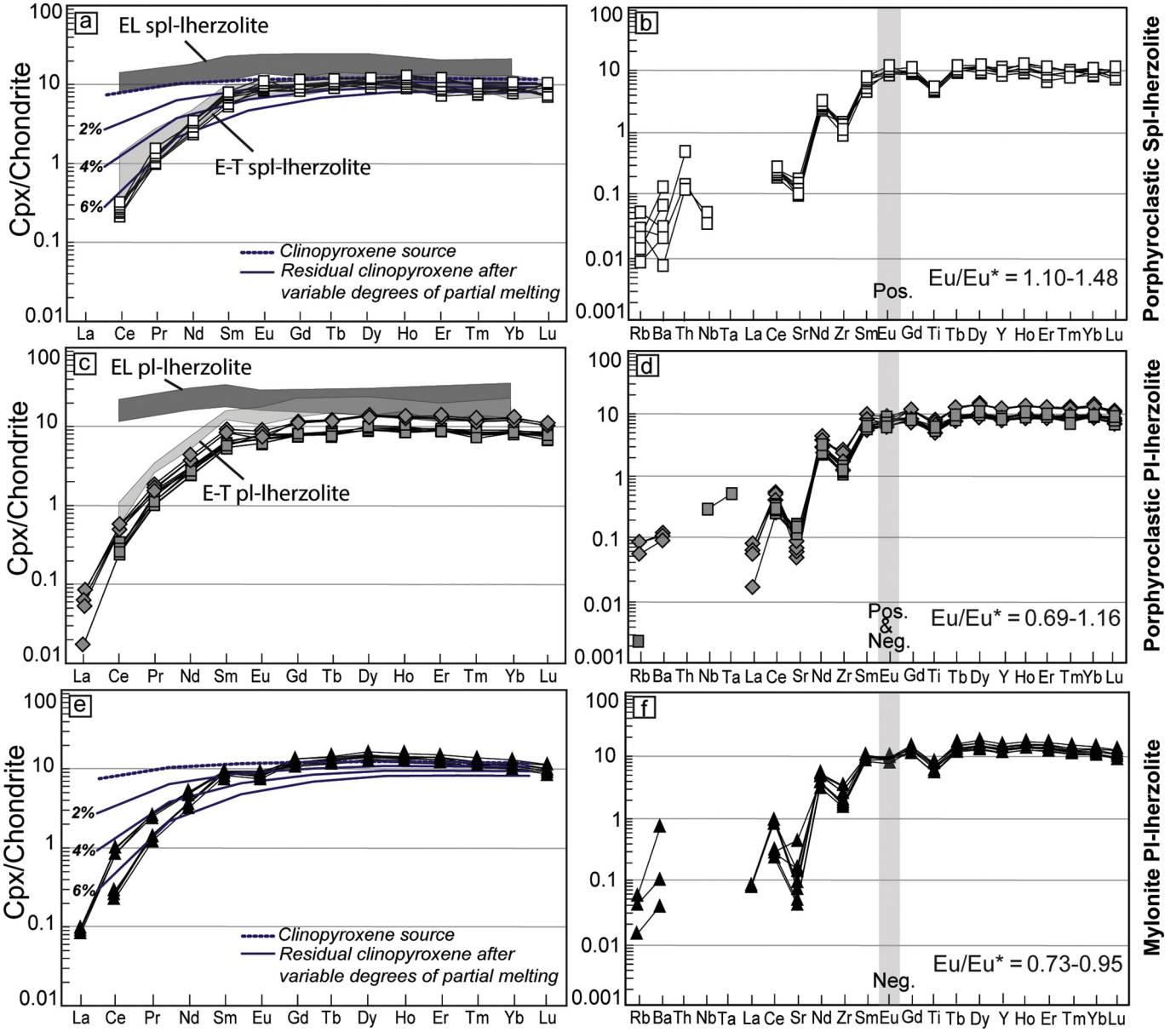

Fig. 9. Chondrite-normalized (a, c, and e) REE and (b, d, and f) multi-element variation diagram patterns for clinopyroxenes from the Nain spinel and plagioclase lherzolites normalized to the chondrite composition of Sun and McDonough (1989). Clinopyroxenes from porphyroclastic spinel lherzolites are shown in (a) and (b), from porphyroclastic plagioclase lherzolites are shown in (c) and (d), and from mylonite plagioclase lherzolites are shown in (e) and (f). Grey fields show the range in clinopyroxene compositions within the External Liguride (EL) and Erro–Tobbio (E–T) spinel and plagioclase lherzolites (Rampone et al., 1993, 1995, 2005). The REE patterns for fractional partial melts derived from spinel peridotite facies (in 1% increments) are also shown, from the source clinopyroxene compositions and melt increments equations of Johnson et al. (1990), the peridotite and melt modes of Kinzler (1997), and the distribution coefficients derived by Suhr et al. (1998). Grey columns highlight Eu values, and positive and negative anomalies are denoted by Pos. and Neg., respectively.

(~0.47 GPa). These calculated pressures correlate to depths of ~20 and ~16 km for the spinel and plagioclase lherzolites, respectively. Unfortunately, the recently proposed geobarometers for plagioclase-bearing mantle rocks (Borghini et al., 2010, 2011; Fumagalli et al., 2017) can only be used for plagioclase lherzolite sample 88 and the mylonites as a result of the lack of fresh plagioclase in the other samples. Sample 88 yielded an estimated pressure of 0.37 GPa using the Borghini et al. (2010) method and 0.53 GPa using the Fumagalli et al. (2017) method. The pressure estimate obtained using the Fumagalli et al. (2017) method is similar to that obtained using the Nimis and Ulmer (1998) barometer (0.49 GPa). Mylonite pressure estimates vary as a function of the method used (Table 2), with a mean equilibration pressure of 0.42 GPa. All of these estimated temperatures and pressures fall within the stability field of pargasite (Jenkins, 1983), and the highest lherzolite temperatures are close to 900 °C, which is the temperature of the upper thermal stability of pargasite coexisting with orthopyroxene (Lykins and Jenkins, 1992).

9. Discussion

9.1. Mantle metasomatism: evidence from depleted amphibole compositions

The lherzolites are slightly depleted as a result of low-degree partial melting that likely preceded amphibole metasomatism. In fact, the REE normalized patterns of the spinel lherzolites are consistent with patterns calculated for a fertile mantle source that had undergone low-degree fractional partial melting (~5%; Fig. 12a). This is also consistent with the compositions of spinel and clinopyroxene within these lherzolites (Figs. 3 and 9a; Supplementary Table 2). The presence of pargasite in both spinel and plagioclase lherzolites suggests that

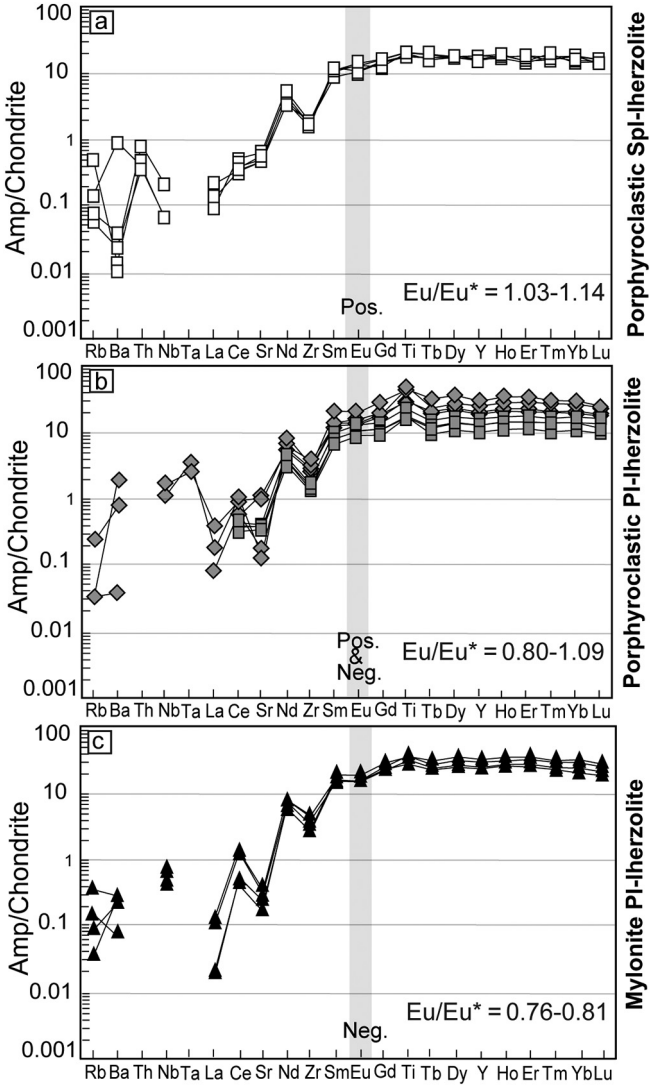

Fig. 10. Chondrite-normalized multi-element variation diagram patterns for amphiboles from the Nain spinel and plagioclase lherzolites normalized to the chondrite composition of Sun and McDonough (1989). Amphiboles from porphyroclastic spinel lherzolites are shown in (a), from porphyroclastic plagioclase lherzolites are shown in (b), and from mylonite plagioclase lherzolites in (c). Grey columns highlight Eu values, and positive and negative anomalies are denoted by Pos. and Neg., respectively.

metasomatism associated with the formation of this mineral preceded the formation of plagioclase, indicating that the crystallization of the plagioclase was not associated with this metasomatic event. The pargasite in the studied rocks contains very low concentrations of the LREE and the large ion lithophile elements (LILE; Fig. 10a–c; Supplementary Tables 5 and 9), which indicates that this mineral has a refractory nature. Amphiboles with similarly depleted compositions are uncommon in mantle rocks (e.g., Menzies and Hawkesworth, 1987), but have been identified within fertile subcontinental-type lherzolites (e.g., Chazot et al., 2005; Green, 1964; Hoogerduijn Strating et al., 1993; Piccardo et al., 1993; Rampone et al., 1993, 1995; Zanetti et al., 1996, 2000) and in some mantle xenoliths (e.g., Abe et al., 1998; Arai, 1986; Johnson et al., 1996). Two major processes explain the presence of depleted amphiboles in mantle peridotites: (i) re-equilibration with depleted pyroxenes; (ii) metasomatism by H_2O-rich mantle fluids. The first hypothesis suggests that these amphiboles were originally enriched in the LREE and the LILE but became depleted as a result of the sub-solidus redistribution of elements between amphiboles and depleted pyroxenes within the hosting peridotite (Vannucci et al., 1995; Zanetti et al., 1996). The similar REE patterns of pargasite and clinopyroxene (Figs. 9a, 10a, 13) indicate that these minerals are in equilibrium within the Nain lherzolites. This suggests that originally enriched amphiboles have equilibrated with coexisting and rather depleted clinopyroxenes. However, the composition of the initial amphibole within the lherzolites is unknown, meaning that it is not possible to quantitatively model this amphibole–clinopyroxene re-equilibration. Nevertheless, given the very depleted nature of the studied pargasites and assuming an original amphibole with enriched composition, it follows that, in order to compensate the enriched composition of the amphibole, the composition of the original clinopyroxene should have been very depleted. However, a very depleted composition of the original clinopyroxene implies that the hosting peridotites experienced high-degree partial melting (>20%). Nevertheless, this hypothesis is in contrast with both the mineral and whole-rock geochemistry of the Nain spinel lherzolites, which is indicative of ~5% fractional melting (Figs. 3, 9a, 12a; Supplementary Table 2). Therefore, the depleted composition of the amphiboles in these units was not influenced by re-equilibration with clinopyroxene.

The second hypothesis suggests that the depleted amphiboles were derived from low-density H_2O-rich metasomatic fluids that were originally depleted in incompatible elements. In turn, the LREE-depleted character of these aqueous fluids is interpreted to be the result of the earlier equilibration of these fluids in the garnet stability field, as suggested for the genesis of depleted amphiboles within the External Liguride and Zabargad peridotites (e.g., Piccardo et al., 1993; Rampone et al., 1993; Vannucci et al., 1995). The hypothetical metasomatic fluids that interacted with the Nain lherzolites are likely to have had flat HREE and slightly depleted LREE patterns (mean $Ce_N/Yb_N = 0.10–0.13$; Fig. 13). The REE concentrations of these metasomatic fluids can be modeled using clinopyroxene–amphibole/basaltic melt partition coefficients (Hart and Dunn, 1993; Sisson, 1994). This modelling suggests that the metasomatic agents were subalkaline mafic melts that closely resemble the tholeiitic melts in slow-spreading-ridge settings such as the Mid-Atlantic Ridge (e.g., Sun et al., 1979; Fig. 13b). The water content of these metasomatic melts was likely supplied by degassing of deeper parts of the mantle during the initial stages of basin extension. The depleted chemistry of these amphiboles suggests that metasomatism occurred either after or contemporaneously with the partial melting of the lherzolites. In summary, it is likely that the depleted chemistry of the Nain pargasites is the result of metasomatism by H_2O-rich mantle fluids.

9.2. Positive Eu anomalies in mantle clinopyroxene

The REE patterns of clinopyroxene within the spinel lherzolites are similar to the calculated composition of clinopyroxene after low-degree (≤5%) partial melting (Fig. 9a), with the exception of the slight to appreciable positive Eu anomalies within the clinopyroxenes ($Eu/Eu^* = 1.10–1.48$; Fig. 9b; Supplementary Table 8). Similar positive anomalies are also present within coexisting amphiboles ($Eu/Eu^* = 1.03–1.14$) and orthopyroxenes ($Eu/Eu^* = 1.01–1.69$; Figs. 8b, 10a; Supplementary Tables 7 and 9). These positive Eu anomalies, although slight, are remarkable, as Eu behaves incompatibly during mantle melting (e.g., Sun and Liang, 2012). This means that pyroxenes within residual mantle material typically have negative Eu anomalies (e.g., Tang et al., 2017). The unusually high concentrations of Eu in the studied clinopyroxenes can be explained in two ways, as outlined below.

The first hypothesis is based on the heterovalent state of Eu, which is the only REE that can exist in divalent and trivalent states under magmatic conditions. This means that the Eu mineral/melt partition coefficient for a given mineral is dependent on Eu^{3+}/Eu^{2+} ratios that in turn are predominantly a function of the prevailing redox conditions. Although few experimental studies have considered the partitioning of Eu in mantle minerals as a function of oxygen fugacity conditions,

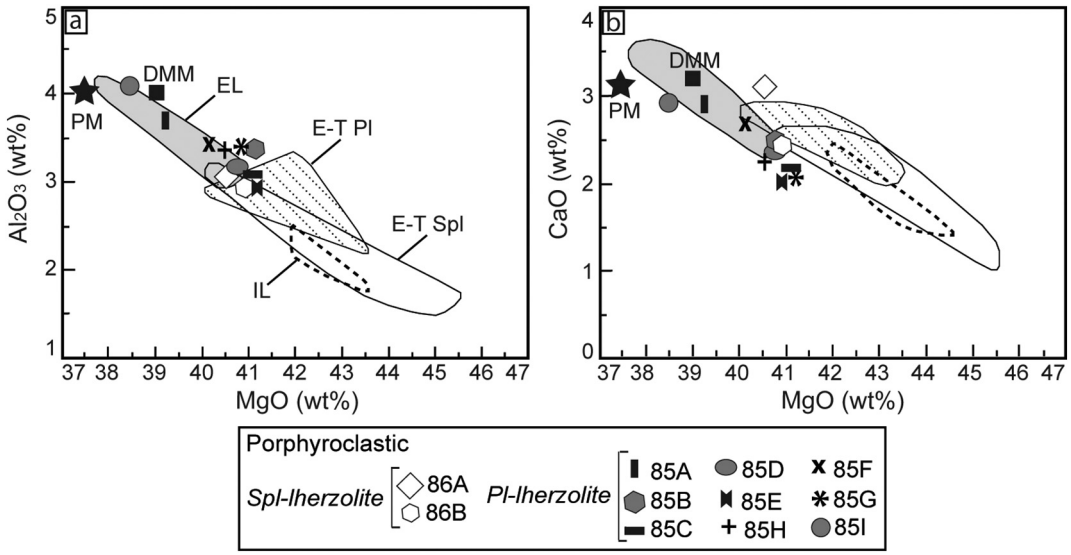

Fig. 11. Al_2O_3 (a) and CaO (b) versus MgO diagrams for mantle lherzolites from the Nain ophiolitic complex compared with variations in mantle peridotites from the Internal (Rampone et al., 1998) and External (Ottonello et al., 1984; Rampone et al., 1993, 1995) Ligurides of the northern Apennines and the Erro–Tobbio ophiolites in the Ligurian Alps (Rampone et al., 2005). The compositions of the depleted MORB mantle (DMM) and the primitive mantle (PM) are from Workman and Hart (2005) and Sun and McDonough (1989), respectively.

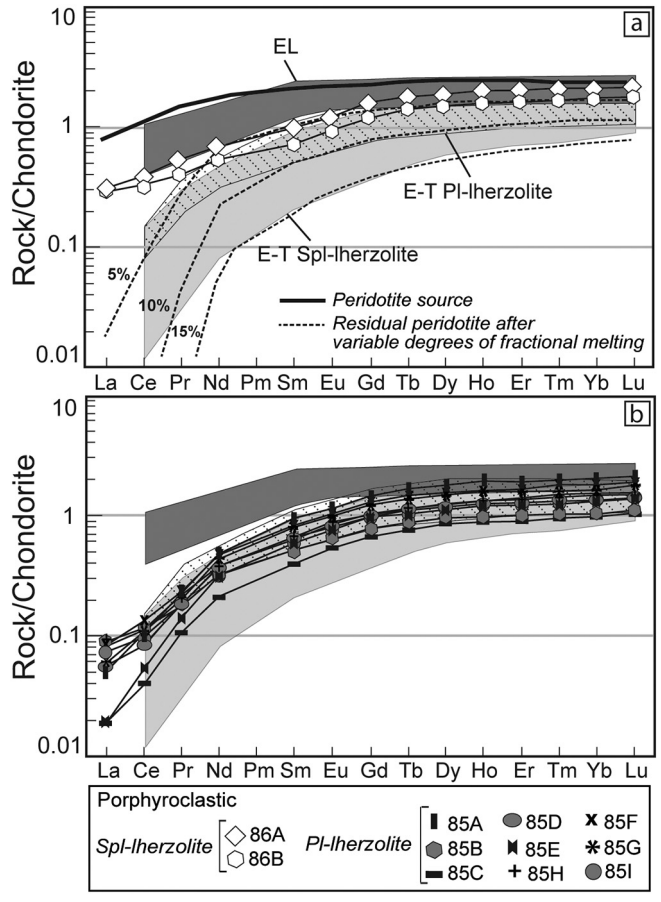

Fig. 12. Chondrite-normalized REE compositions of mantle lherzolites from the Nain ophiolitic complex normalized to the chondrite composition of Sun and McDonough (1989). Grey and dashed fields show the bulk-rock compositions of peridotites from the External Liguride (EL) and Erro–Tobbio (E–T) ophiolites, respectively (Rampone et al., 1993, 1995, 2005). Also shown are calculated depletion curves derived using fractional melting models by Niu and Hékinian (1997), which used source peridotite compositions with comparable modal compositions to that of the Nain spinel lherzolites.

the results show a positive correlation between oxygen fugacity and pyroxene Eu partition coefficient values (e.g., Karner et al., 2010; Laubier et al., 2014; McKay, 2004; Möller and Muecke, 1984; Schwandt and McKay, 1998; Sun et al., 1974; Weill and McKay, 1975). The oxygen fugacity conditions recorded by the spinel lherzolites (Table 2) vary between fayalite–magnetite–quartz (FMQ) −0.8 and FMQ +1.3, clearly indicating oxidizing conditions (e.g., Ballhaus et al., 1990, 1991). This suggests that the unusually positive Eu anomalies within the clinopyroxenes were generated by the partial melting of lherzolites under oxidizing conditions, favoring the retention of Eu within clinopyroxene. The second hypothesis involves the generation of positive Eu anomalies within these clinopyroxenes by the sequestering of Eu from the plagioclase that was originally present within these rocks. This implies that the studied spinel lherzolites are likely to have been derived from earlier-formed plagioclase lherzolites that are not preserved within the Nain mantle series. The precursor plagioclase most likely formed by the crystallization of trapped melts in the lherzolites that were produced in situ during partial melting. The breakdown of plagioclase during the transition from plagioclase to spinel facies caused the clinopyroxene within these rocks to incorporate the excess Eu that was originally hosted by plagioclase. The shape of the pressure (P)–temperature (T) curve that separates the spinel and plagioclase facies in the mantle (e.g., Irving and Green, 1970; Kushiro and Yoder, 1966) suggests that the transition from the latter to the former can be achieved by a simple temperature decrease at almost constant pressure. Both of the hypotheses discussed above can explain the positive Eu anomalies within the clinopyroxenes in the studied rocks, although the data obtained to date do not allow a further assessment of the specific process that generated these Eu anomalies.

Positive Eu anomalies are also present in some pyroxene and amphibole cores within the studied plagioclase lherzolites although the majority of these minerals have negative Eu anomalies (Supplementary Tables 7–9). This change in Eu anomaly is most likely related to the subsolidus recrystallization of spinel to plagioclase, note the plagioclase within the plagioclase lherzolites represents a different generation of plagioclase formation and is not related to the postulated “magmatic” plagioclase discussed above.

Table 2
Calculated equilibration temperatures, pressures, and oxygen fugacity conditions for the Nain spinel and plagioclase lherzolites.

Texture	Rock type	Rock no.	T (°C) Ca in Opx	T (°C) 2-pyrox	T (°C) Ca in Opx	T_{REE} (°C) 2-pyrox	P (GPa) Ca in Cpx	P(GPa) An in Pl	P(GPa) pl and 2-pyrox	fO_2 (FMQ)
			Brey and Köhler (1990)		Witt-Eickschen and Seck (1991)	Liang et al. (2013)	Nimis and Ulmer (1998)	Borghini et al. (2011)	Fumagalli et al. (2017)	Ballhaus et al. (1990)
Porphyroclastic	Spl-lherzolite	83	834 ± 29	842 ± 25	928 ± 26	1064 ± 62	0.60			−0.78
		86-A	939 ± 22	888 ± 36	935 ± 28		0.60			0.74
		86-B	921 ± 17	937 ± 28	938 ± 24		0.60			1.25
	Pl-lherzolite	85	845 ± 26	907 ± 22	906 ± 28	1017 ± 45	0.56			−1.16
		88	823 ± 28	925 ± 16	911 ± 17	1059 ± 58	0.49	0.37	0.53	−0.39
		85B	914 ± 31	873 ± 29	941 ± 12		0.49			0.46
		85D	923 ± 27	910 ± 23	937 ± 16		0.42			
		85F	918 ± 22	885 ± 31	930 ± 12		0.49			0.61
		85G	899 ± 25	882 ± 31	939 ± 9		0.46			
		85H	924 ± 28	909 ± 29	933 ± 22		0.44			0.46
		85I	904 ± 31	927 ± 17	935 ± 14		0.44			0.42
Mylonitic	Pl-lherzolite	50	887 ± 16	891 ± 20	886 ± 21	1029 ± 23	0.40	0.37	0.49	
		51	877 ± 18	899 ± 15	893 ± 19	1019 ± 52	0.38	0.39	0.50	

Footnote: equilibrium pressure was assumed to be 1 GPa for temperature calculations using the approach of Brey and Köhler (1990). Pyroxenes are denoted by Pyrox with all other abbreviations as in Fig. 2. Oxygen fugacities are expressed relative to the fayalite–magnetite–quartz (FMQ) oxygen buffer, and the data represent mean values for each sample (n > 5).

9.3. Metamorphic evolution of the lherzolites: recrystallization in the plagioclase facies and mylonitization

9.3.1. Microtextural evidence

The studied plagioclase lherzolites are characterized by: (i) the development of plagioclase rims around spinel as well as around spinel inclusions within pyroxene porphyroclasts (Fig. 2c, e, f); (ii) the development of plagioclase + orthopyroxene exsolution lamellae in some clinopyroxene porphyroclasts (Fig. 2g); (iii) a noticeable decrease in modal pyroxenes abundances as modal olivine and plagioclase abundances increase (Table 1). Similar microtextures are present in plagioclase peridotites from the northern Apennines, western Iberia, and on Zabargad Island, where they are interpreted to be the result of the re-equilibration of peridotites under conditions of the plagioclase facies (e.g., Chazot et al., 2005; Kornprobst and Tabit, 1988; Piccardo et al., 1993; Rampone et al., 1993, 1995, 2005). The progressive increase in the degree of recrystallization in the plagioclase facies is associated with an increase in modal plagioclase abundance within the lherzolites (Table 1). The spinel assemblage within both plagioclase and spinel lherzolites is almost identical in texture and chemistry (Figs. 3–6; Supplementary Tables 2–4). This also supports the hypothesis that the plagioclase lherzolites were generated by the recrystallization of pre-existing spinel lherzolites. Similarly, comparing these features indicates a genetic link between the porphyroclastic and mylonitic peridotites, whereby the latter were formed by the deformation of the former.

The textural features of the Nain peridotites are different from the textures present within melt-impregnated peridotites. In particular, specific microtextures associated with melt–rock interaction that are typically observed within plagioclase-impregnated peridotites are absent from the Nain lherzolites. These include the presence of gabbroic or plagioclase veinlets/pockets that cut the peridotite matrix or porphyroclasts and the co-crystallization of plagioclase and pyroxene from the impregnating melts (e.g., Dijkstra et al., 2001; Piccardo and Vissers, 2007; Pirnia et al., 2010; Rampone et al., 1997, 2008; Rampone and Borghini, 2008; Susini and Wezel, 1999; Tartarotti et al., 2002). This contrasts with the negative correlation between modal plagioclase and pyroxene abundances within the Nain lherzolites (Table 1). A few discrete plagioclase crystals that could eventually be associated with melt impregnation processes are present within the mylonites (Fig. 2j). However, the overall textural evidence indicates that these plagioclase crystals have been separated from their associated spinels and have recrystallized as individual grains due to foliation in the mylonite matrix.

9.3.2. Mineral compositional evidence

The spinel within the plagioclase peridotites records specific chemical features that are the result of chemical re-equilibration between spinel and plagioclase. These chemical features include being depleted in Al and enriched in Cr, Ti, and Fe, and are generally present in both recrystallized and melt-impregnated peridotites (e.g., Chazot et al., 2005; Dick and Bullen, 1984; Dijkstra et al., 2001; Loocke and Snow, 2013; Piccardo et al., 2004; Rampone et al., 1995, 2008; Tartarotti et al., 2002). However, the chemistry of the spinels is slightly different in the two groups of peridotites (Figs. 4, 5). In particular, a comparison between the chemical features of spinels and those of coexisting minerals (i.e., olivine), may reveal different chemical patterns within recrystallized and melt-impregnated peridotites (Fig. 3).

The Nain plagioclase lherzolites contain chemically zoned spinel (Figs. 4, 5; Supplementary Table 2) where Al and Ni concentrations decrease and Cr, Ti, and Fe concentrations increase from core to rim. The intensity of this zonation is proportional to the modal abundance of plagioclase within these lherzolites (Figs. 4, 5; Table 1; Supplementary Table 2). The Al depletions and Cr, Ti, and Fe enrichments can be explained by the equilibration of these spinels with plagioclase (e.g., Chazot et al., 2005; Dick and Bullen, 1984; Dijkstra et al., 2001; Loocke and Snow, 2013; Piccardo et al., 2004; Rampone et al., 1995, 2008; Tartarotti et al., 2002). However, the Ni depletions are the result of

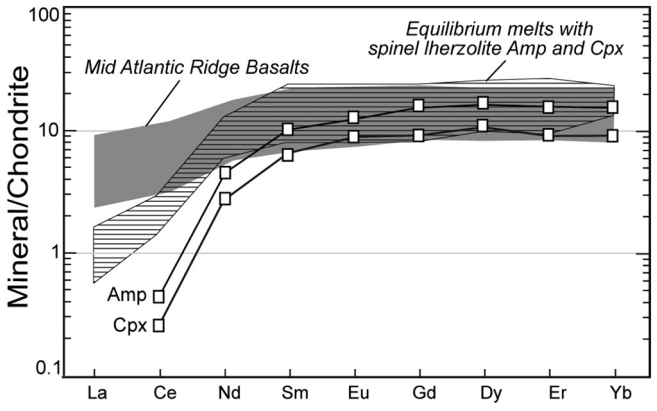

Fig. 13. Chondrite-normalized REE compositions of the calculated metasomatic melts that interacted with the Nain spinel lherzolites, normalized to the chondrite composition of Sun and McDonough (1989). The Mid-Atlantic basalt field is from Sun et al. (1979) and the partition coefficients that were used to calculate equilibrium melts are from Sisson (1994) and Hart and Dunn (1993).

chemical exchange between spinel and coexisting olivine (e.g., Okamura et al., 2006). The crystallization of olivine with plagioclase as a result of subsolidus reactions (e.g., Kushiro and Yoder, 1966) promoted the extraction of Ni from coexisting spinel within these lherzolites. All these zonations are present in spinels associated with olivines with almost uniform Fo contents (Fig. 3; Supplementary Table 1), in contrast to the chemical variations recorded in spinel and olivine within melt-impregnated peridotites, where olivine Fo contents show a marked decrease with increasing degree of melt impregnation (Fig. 3). In addition, the spinel in the studied lherzolites has higher Ti contents (mean of 0.22 wt%) for the same range of Cr# values than spinel within melt-impregnated abyssal peridotites (mean of 0.10 wt%; Fig. 5; Supplementary Table 2). The Ti-rich nature of these spinels indicates that the lherzolites are fertile, providing evidence of a subsolidus rather than magmatic origin for the plagioclase.

The spinels have lower Mg# values than spinels from melt-impregnated peridotites (Fig. 4), indicating that the former record lower equilibration temperatures than the latter (Table 2). The decrease in Mg# from core to rim in the spinels (Fig. 4; Supplementary Table 2) can also be explained by cooling (see Arai, 1992). In addition, an increase in the modal abundance of olivine could promote the exchange of Mg from spinel to coexisting olivine, explaining why spinels within plagioclase lherzolites containing higher modal abundances of olivine (Table 1) have lower Mg# values (mean of 0.74) than spinels within spinel lherzolites (mean of 0.69; Fig. 4; Supplementary Table 2). The fine grain size of the minerals within the mylonites most likely favored the processes that control the redistribution of Mg between spinel and olivine, as described above. This means that for a given Cr#, the spinels within the mylonites have lower Mg# values (mean of 0.65) than those in the porphyroclastic lherzolites (Fig. 4; Supplementary Table 2).

The pyroxenes within the lherzolites are chemically zoned, where Al and Ca decrease from core to rim (Fig. 6c–f; Supplementary Tables 3 and 4) as a result of a combination of cooling and plagioclase crystallization. These lherzolites re-equilibrated under P–T conditions of the plagioclase facies (823 °C–941 °C, 0.47 GPa), causing the solubility of Al and Ca (Tschermak's molecules, $CaAl_2SiO_6$) within these pyroxenes to decrease (e.g., Witt-Eickschen and Seck, 1991). The crystallization of plagioclase had a similar effect on these pyroxenes, as both of these elements are also highly compatible in plagioclase. The pyroxenes within plagioclase-rich lherzolites have mean Al and Ca concentrations that are lower than the concentrations of these elements in pyroxenes within plagioclase-poor lherzolites, despite the fact that these pyroxenes have similar Mg# values (Fig. 6a, b; Supplementary Tables 3 and 4). In addition, pyroxene cores in contact with plagioclase inclusions have low Al and Ca contents (Supplementary Table 3). Pyroxene Ti and Cr concentrations are similar to spinel Ti and Cr concentrations in that they increase with increasing modal plagioclase abundance (Fig. 6a–d; Table 1; Supplementary Tables 3 and 4). The clinopyroxenes contain higher concentrations of Ti than those within melt-impregnated peridotites containing spinels with comparable compositions (Fig. 14). These relatively high clinopyroxene Ti concentrations indicate that the lherzolites are fertile rather than reflecting any melt interactions. The pargasites show similar major-element compositional variations to the pyroxenes, where decreases in Al, Ca, and Na and increases in Ti and Cr are associated with an increase in modal plagioclase abundance (Table 1; Fig. 7; Supplementary Table 5). The lherzolites display a clear positive correlation between modal plagioclase abundance and the concentrations of trace elements in pyroxenes and pargasites barring Eu and Sr, both of which slightly decrease with increasing modal plagioclase abundance (Table 1; Supplementary Tables 7–9). This increase in trace element concentrations associated with the increase in degree of recrystallization generated slightly more enriched pyroxenes and pargasites in the porphyroclastic plagioclase lherzolites than in the spinel lherzolites (Figs. 8a–d, 9a–d, 10a, b). The breakdown of pyroxene and pargasite as a result of subsolidus reactions provided excess REE and LILE to the lherzolite matrix. These trace elements were subsequently taken up by the newly formed plagioclase and the remaining pyroxene and pargasite. This means that the pyroxene and pargasite within the plagioclase-rich lherzolites has a more fertile chemistry than their counterparts within

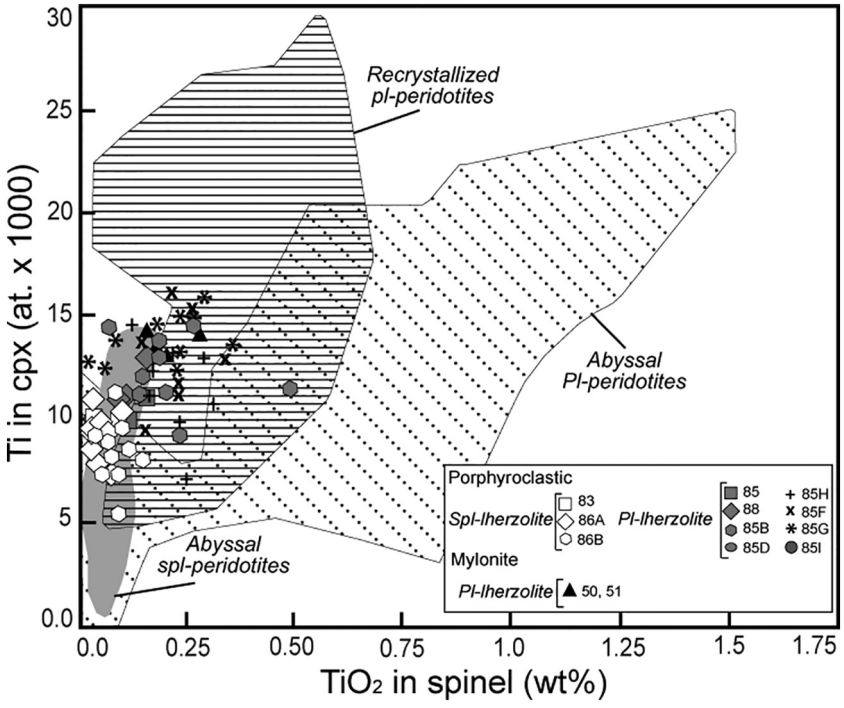

Fig. 14. Ti (in atomic terms × 1000, calculated using six oxygens) in clinopyroxene versus spinel TiO_2 (in wt%) diagram for the Nain plagioclase peridotites compared with compositional fields for abyssal plagioclase peridotites (Dick, 1989; Dick et al., 2010; Seyler and Bonatti, 1997; Susini and Wezel, 1999; Tartarotti et al., 2002) as well as abyssal spinel peridotites (Dick and Bullen, 1984; Seyler and Bonatti, 1997) and recrystallized peridotites (Cannat and Seyler, 1995; Chazot et al., 2005; Hoogerduijn Strating et al., 1993; Montanini et al., 2006; Rampone et al., 1993, 1995, 2005).

the spinel lherzolites (Figs. 8a–d, 9a–d, 10a, b). A similar model has been proposed to explain the composition of plagioclase lherzolites within the External Liguride (Rampone et al., 1993, 1995).

9.3.3. Whole-rock geochemical evidence

Although the Nain spinel and plagioclase lherzolites have significantly different modal compositions, they have similar whole–rock geochemical compositions (Fig. 11; Supplementary Table 10). This similarity supports a metamorphic origin for the plagioclase in these rocks, as the addition of plagioclase by melt impregnation would have increased the concentrations of Al_2O_3, CaO, and TiO_2 in the plagioclase lherzolites relative to the spinel lherzolites (e.g., Rampone et al., 2008; Seyler and Bonatti, 1997; Susini and Wezel, 1999). In addition, the plagioclase lherzolites contain similar concentrations of the HREE and have similar MREE/HREE ratios relative to the spinel lherzolites ($Sm_N/Yn_N = 0.41–0.50$ for the plagioclase lherzolites, 0.41–0.46 for spinel lherzolites). However, the plagioclase lherzolites contain lower concentrations of the LREE than the spinel lherzolites, reflecting the lower modal abundances of pyroxene in the former relative to the latter (Fig. 12; Supplementary Table 10).

10. Geodynamic implications

The Nain ophiolites are thought to have formed in either (i) a Cretaceous continental volcanic arc related to the eastward subduction of a narrow branch of the Tethyan Ocean crust under the CEIM (e.g., Delaloye and Desmons, 1980; Desmons, 1982; Desmons and Beccaluva, 1983; Ghazi and Hassanipak, 2000); or (ii) a Late Cretaceous ensimatic backarc extensional basin that formed to the north of the Sanandaj–Sirjan as a result of the subduction of the southern Neotethyan Basin associated with the formation of the Zagros fold–thrust belt (e.g., Pirnia et al., 2010; Shafaii Moghadam et al., 2009; Shahabpour, 2005). However, both these tectonic reconstructions focus on the convergent and oceanic closure phases of the evolution of this region, meaning that the tectonic setting during oceanic basin opening remains unclear. The mantle lherzolites that crop out in the Nain ophiolites have mineral (e.g., Fig. 9) and whole-rock (Figs. 11, 12) geochemical compositions that typify subcontinental mantle material exhumed at Iberia-type (i.e., magma-poor or Alpine-type) rifted continental margins (Rampone et al., 1995, 2005; Saccani et al., 2013, 2015). The classical models proposed for the magma-poor rifted margins of the western Tethys (for a general review and relevant references, see Dilek and Furnes, 2011; Saccani et al., 2015) suggest that the CEIM was rifted from the continental block of Central-West Iran as a result of asymmetrical passive extension. This tectonism caused the exhumation of subcontinental mantle now recorded in the Nain lherzolites. These lherzolites record low-degree partial melting (<5%; Fig. 12), suggesting that this region was similar to the western Tethys in that the upwelling and exhumation of subcontinental mantle in the Nain area was associated with limited partial melting and limited magmatism, processes that are typically associated with magma-poor rifted margins (Saccani et al., 2015).

Unfortunately, the age of continental rifting and subsequent seafloor spreading in the study area cannot be accurately defined. However, Lensch and Davoudzadeh (1982) used the regional scale geology to suggest that this area records Triassic to Jurassic rifting around the Central and East Iran blocks that separate the CEIM from neighboring continental blocks. In addition, Berberian and King (1981) suggested that extensional movements around the CEIM occurred in the Late Triassic. Paleomagnetic data indicate that the CEIM drifted southward and underwent a counterclockwise rotation in Middle Jurassic-Early Cretaceous. During this period, oceanic crust was forming all around the CEIM (e.g., Mattei et al., 2014, and references therein). These data suggest that the continental rifting in this region and the associated exhumation of the Nain subcontinental lherzolites occurred no later than the Late Triassic to Early Jurassic. Our reconstruction indicates that the Nain subcontinental mantle lherzolites are genetically and temporally unrelated to mantle harzburgites (and associated dunites and chromitite pods) and the Late Cretaceous volcanic arc-type magmatic rocks that crop out in the Nain mélange (e.g., Desmons and Beccaluva, 1983; Ghazi and Hassanipak, 2000; Khalatbari-Jafari et al., 2015; Shafaii Moghadam et al., 2009). In fact, the Nain subcontinental mantle lherzolites originally represented the western border of the CEIM or alternatively the neighboring OCTZ. This means that the Nain ophiolites can be classified as Continental Margin ophiolites according to recent ophiolite classifications (e.g., Dilek and Furnes, 2011; Saccani, 2015; Saccani et al., 2015), as they formed during the early stages of ocean basin evolution following continental breakup. In contrast, the mantle harzburgites and the Late Cretaceous volcanic rocks and sheeted dykes that crop out within the Nain mélange represent typical volcanic arc-type ophiolites. These two different ophiolite suites were tectonically incorporated into the colored mélange and were then emplaced onto the central Iran continental margin during convergence and subsequent continental collision in the Late Cretaceous.

11. Summary and conclusions

The Nain lherzolites represent subcontinental mantle peridotites that record the initial stages of oceanic basin formation around the CEIM. The subcontinental nature of these lherzolites is suggested by chemical and textural similarities with subcontinental peridotites in magma-poor (Iberia-type) continental margin ophiolites. These similarities include the fact that the Nain lherzolites are relatively fertile, recording only ~5% partial melting that likely occurred during their exhumation from asthenospheric to lithospheric levels in response to continental rifting and lithospheric extension. The slight to significant positive Eu anomalies in pyroxenes and pargasite within spinel lherzolites in this area are the result of partial melting under high oxygen fugacity. The oxygen fugacity calculated for these spinel lherzolites varies between FMQ −0.8 and FMQ +1.3. The depleted chemistry of the pargasites suggests that the metasomatic agents that interacted with the Nain lherzolites were low-density aqueous melts that were originally chemically depleted. These melts were tholeiitic and had compositions similar to those of melts generated at slow spreading centers. The depleted nature of the pargasites in this region suggests that metasomatism occurred contemporaneous with or after the partial melting recorded within these lherzolites. The further accretion of lherzolites into the lithosphere and lower depths was associated with their ascent from conditions of the mantle spinel facies to those of the mantle plagioclase facies. The recrystallization of these lherzolites under plagioclase facies conditions is recorded by textural and mineral chemical evidence, including: (1) the development of plagioclase rims around spinel; (2) the presence of plagioclase + orthopyroxene exsolution lamellae within clinopyroxene porphyroclasts; (3) a positive correlation between plagioclase modal abundances and olivine modal abundances, and a negative correlation between plagioclase modal abundances and pyroxene modal abundances; (4) decreases in Al, Mg, and Ni, and increases in Cr, Ti, and Fe concentrations in spinel; (5) decreases in Al and Ca, and increases in Cr and Ti concentrations in pyroxenes and pargasite; and (6) a slight overall increase in the concentration of the REE and the majority of the trace elements (barring Eu and Sr, which slightly decrease) in pyroxenes and pargasite.

Acknowledgments

The first author was supported during this research by a MARIE SKŁODOWSKA-CURIE project CIAO (project number 658591). We thank Dr. G. Torabi for assistance during fieldwork, Drs T. Tamura and A. Zanetti for assistance during LA–ICP–MS analysis, and Dr. F. Zaccarini for assistance during electron microprobe analysis. We also thank Profs Dante Canil and Elisabetta Rampone for constructive comments, and Prof. Andrew Kerr for editorial handling and helpful suggestions.

Appendix A. Supplementary data

Supplementary data to this article can be found online at https://doi.org/10.1016/j.lithos.2018.04.001.

References

Abe, N., Arai, S., Yurimoto, H., 1998. Geochemical characteristics of the uppermost mantle beneath the Japan island arcs: implications for upper mantle evolution. Physics of the Earth and Planetary Interiors 107, 233–248.

Arai, S., 1984. Igneous mineral equilibria in some alpine-type peridotites in Japan. In: Sunagawa, I. (Ed.), Material Science of the Earth's Interior. Terra Scientific Publication, Tokyo, Japan, pp. 445–460.

Arai, S., 1986. K/Na variation in phlogopite and amphibole of upper mantle peridotites due to fractionation of the metasomatizing fluids. Journal of Geology 94, 436–444.

Arai, S., 1992. Chemistry of chromian spinel in volcanic rocks as a potential guide to magma chemistry. Mineralogical Magazine 56, 173–184.

Arai, S., 1994. Characterization of spinel peridotites by olivine spinel compositional relationships: reviews and interpretation. Chemical Geology 111, 191–204.

Arvin, M., Robinson, P., 2011. The petrogenesis and tectonic setting of lavas from the Baft ophiolitic mélange, southwest of Kerman, Iran. Canadian Journal of Earth Sciences 31, 824–834.

Ballhaus, C., Berry, R.F., Green, D.H., 1990. Oxygen fugacity controls in the Earth's upper mantle. Nature 349, 437–440.

Ballhaus, C., Berry, R.F., Green, D.H., 1991. High pressure experimental calibration of the olivine-orthopyroxene-spinel oxygen geobarometer: implications for the oxidation state of the upper mantle. Contributions to Mineralogy and Petrology 107, 27–40.

Berberian, M., King, G.C.P., 1981. Towards a Paleogeography and Tectonic Evolution of Iran. 18. National Research Council of Canada, pp. 210–265.

Borghini, G., Fumagalli, P., Rampone, E., 2010. The stability of plagioclase in the upper mantle: subsolidus experiments on fertile and depleted lherzolite. Journal of Petrology 51, 229–254.

Borghini, G., Fumagalli, P., Rampone, E., 2011. The geobarometric significance of plagioclase in mantle peridotites: a link between nature and experiments. Lithos 126, 42–53.

Brey, G.P., Köhler, T., 1990. Geothermobarometry in four-phase lherzolites II. New thermobarometers, and practical assessment of existing thermobarometers. Journal of Petrology 31, 1353–1378.

Canil, D., Johnston, S.T., Evers, K., Shellnutt, J.G., Creaser, A., 2003. Mantle exhumation in an early Paleozoic passive margin, northern Cordillera, Yukon. Journal of Geology 111, 313–327.

Cannat, M., Seyler, M., 1995. Transform tectonics, metamorphic plagioclase and amphibolitization in ultramafic rocks of the Vema transform fault (Atlantic Ocean). Earth and Planetary Science Letters 133, 283–298.

Cannat, M., Chatin, F., Whitechurch, H., Ceuleneer, G., 1997. Gabbroic rocks trapped in the upper mantle at the mid-Atlantic ridge. Proceeding of the Ocean Drilling Program, Scientific Results 153, 243–264.

Chazot, G., Charpentier, S., Kornprobst, J., Vannucci, R., Luais, B., 2005. Lithospheric mantle evolution during continental break-up: the west Iberia non-volcanic passive margin. Journal of Petrology 46, 2527–2568.

Constantin, M., 1999. Gabbroic intrusions and magmatic metasomatism in harzburgites from the Garratt transform fault: implications for the nature of mantle–crust transition at fast-spreading ridges. Contributions to Mineralogy and Petrology 136, 111–130.

Davoudzadeh, M., 1972. Geology and petrology of the area north of Nain, Central Iran. Geological Survey of Iran, Report No. 1, p. 89.

Delaloye, M., Desmons, J., 1980. Ophiolites and mélange terranes in Iran: a geochronological study and its paleotectonic implications. Tectonophysics 68, 83–111.

Desmons, J., 1982. Meso-Cainozoic palaeogeography of the Middle East: constraints from the Iranian sutures. Géologie Alpine 58, 21–30.

Desmons, J., Beccaluva, L., 1983. Mid-Ocean ridge and island-arc affinities in ophiolites from Iran: palaeographic implications. Chemical Geology 39, 39–63.

Dick, H.J.B., 1989. Abyssal peridotites, very slow spreading ridge and ocean ridge magmatism. In: Sanders, A.D., Norry, M.J. (Eds.), Magmatism in the Ocean Basins. Geological Society, London, Special Publication vol. 42, pp. 71–105.

Dick, H.J.B., Bullen, T., 1984. Chromian spinel as a petrogenetic indicator in abyssal and alpine-type peridotites and spatially associated lavas. Contributions to Mineralogy and Petrology 86, 54–76.

Dick, H.J.B., Lissenberg, C.J., Warren, J.M., 2010. Mantle melting, melt transport, and delivery beneath a slow-spreading ridge: the paleo-MAR from 23°15′ to 23°45′N. Journal of Petrology 51, 425–467.

Dijkstra, A.H., Drury, M.R., Visser, L.R.M., 2001. Structural petrology of plagioclase peridotite in the West Othris Mountains (Greece): melt impregnation in mantle lithosphere. Journal of Petrology 42, 5–24.

Dilek, Y., Furnes, H., 2011. Ophiolite genesis and global tectonics: geochemical and tectonic fingerprinting of ancient oceanic lithosphere. Geological Society of America Bulletin 123, 387–411.

Dilek, Y., Moores, E.M., Delaloye, M., Karson, J.A., 1991. Amagmatic extension and tectonic denudation in the Kizildag ophiolite, southern Turkey: implications for the evolution of Neotethyan oceanic crust. In: Peters, Tj, et al. (Eds.), Ophiolite Genesis and Evolution of the Oceanic Lithosphere. Ministry of Petroleum and Minerals, Sultanate of Oman, pp. 485–500.

Droop, G.T.R., 1987. A general equation for estimating Fe^{3+} concentrations in ferromagnesian silicates and oxides from microprobe analyses, using stoichiometric criteria. Mineralogical Magazine 51, 431–435.

Dygert, N., Liang, Y., 2015. Temperature and cooling rates recorded in REE in coexisting pyroxenes in ophiolitic and abyssal peridotites. Earth and Planetary Science Letters 420, 151–161.

Fabries, J., Lorand, J.P., Bodinier, J.P., 1998. Petrogenetic evolution of orogenic lherzolite massifs in the central and western Pyrenees. Tectonophysics 292, 145–167.

Fumagalli, P., Borghini, G., Rampone, E., Poli, S., 2017. Experimental calibration of forsterite-anorthite-Ca-tschermak-enstatite (FACE) geobarometer for mantle peridotites. Contributions to Mineralogy and Petrology 172, 38.

Furusho, M., Kanagawa, K., 1999. Transformation-induced strain localization in a lherzolite mylonite from the Hidaka metamorphic belt of central Hokkaido, Japan. Tectonophysics 313, 411–432.

Ghazi, A.M., Hassanipak, A.A., 2000. Petrology and geochemistry of the Shahr-Babak Ophiolite, central Iran. In: Dilek, Y., Moores, E., Elthon, D., Nicolas, A. (Eds.), Ophiolites and Oceanic Crust; New Insights from Field Studies and the Ocean Drilling Program. Geological Society of America, Special Papers 349, pp. 485–497.

Green, D.H., 1964. The petrogenesis of the high-temperature peridotites intrusion in the Lizard Area, Cornwall. Journal of Petrology 5, 134–188.

Green, D.H., Falloon, T.J., 1998. Pyrolite: a Ringwood concept and its current expression. The Earth's Mantle: Composition, Structure and Evolution. Cambridge University Press, Cambridge, pp. 311–380.

Green, D.H., Hibberson, W., 1970. The instability of plagioclase in peridotite at high pressure. Lithos 3, 209–221.

Green, D.H., Ringwood, A.E., 1970. Mineralogy of peridotitic compositions under upper mantle conditions. Physics of the Earth and Planetary Interiors 3, 359–379.

Hamlyn, P.R., Bonatti, E., 1980. Petrology of mantle-derived ultramafics from the Owen Fracture Zone, Northwest Indian Ocean: implications for the nature of the oceanic upper mantle. Earth and Planetary Science Letters 48, 65–79.

Hart, S.R., Dunn, T., 1993. Experimental cpx/melt partitioning of 24 trace elements. Contributions to Mineralogy and Petrology 113, 1–8.

Hellebrand, E., Snow, J.E., Dick, H.J.B., Hofmann, A.W., 2001. Coupled major and trace elements as indicators of the extent of melting in mid-ocean-ridge peridotites. Nature 410, 677–681.

Hoogerduijn Strating, E.H., Rampone, E., Piccardo, G.B., Drury, M.R., Vissers, R.L.M., 1993. Subsolidus emplacement of mantle peridotites during incipient oceanic rifting and opening of the Mesozoic Tethys (Voltri Massif, NW Italy). Journal of Petrology 34, 901–927.

Irving, A., Green, D.H., 1970. Experimental duplication of mineral assemblages in basic inclusions of the Delegate breccia pipes. Physics of the Earth and Planetary Interiors 3, 385–389.

Jagoutz, E., Palme, H., Badenhausen, H., Blum, K., Candales, M., Dreibus, C., Spettel, B., Lorenz, V., Wanke, H., 1979. The abundances of major and trace elements in the earth's mantle as derived from primitive ultramafic nodules. Proceedings Lunar and Planetary Science Conference. 10, pp. 2031–2050.

Jenkins, D.M., 1983. Stability and composition relations of calcic amphiboles in ultramafic rocks. Contributions to Mineralogy and Petrology 83, 375–384.

Johnson, K.T.M., Dick, H.J.B., Shimizu, N., 1990. Melting in the oceanic upper mantle: an ion microprobe study of diopsides in abyssal peridotites. Journal of Geophysical Research 95, 2661–2678.

Johnson, K.E., Davis, A.M., Bryndzia, L.T., 1996. Contrasting styles of hydrous metasomatism in the upper mantle: an ion microprobe investigation. Geochimica et Cosmochimica Acta 60, 1367–1385.

Kaczmarek, M.A., Müntener, O., 2008. Juxtaposition of melt impregnation and high-temperature shear zones in the upper mantle; field and petrological constraints from the Lanzo peridotite (Northern Italy). Journal of Petrology 49, 2187–2220.

Karner, J.M., Papike, J.J., Sutton, P.V., Burger, P.V., Shearer, C.K., Le, L., Newville, M., Choi, Y., 2010. Partitioning of Eu between augite and a highly spiked Martian basalt composition as a function of oxygen fugacity (IW-1 to QFM): determination of Eu^{2+}/Eu^{3+} ratios by XANES. American Mineralogist 95, 410–413.

Khalatbari-Jafari, M., Sepehr, H., Mobasher, K., 2015. Tectonomagmatic evolution of the South Dehshir Ophiolite, Central Iran. Geological Magazine 153, 557–577.

Kinzler, R.J., 1997. Melting of mantle peridotites at pressure approaching the spinel to garnet transition: application to mid ocean ridge basalt petrogenesis. Journal of Geophysical Research 102, 853–874.

Kornprobst, J., Tabit, A., 1988. Plagioclase-bearing ultramafic tectonites from the Galicia margin (Leg 103, Site 637): comparison of their origin and evolution with low-pressure ultramafic bodies in Western Europe. Proceeding of the Ocean Drilling Program, Scientific Results 103, 253–267.

Kushiro, I., Yoder, H.S., 1966. Anorthite-forsterite and anorthite-enstatite reactions and their bearing on the basalt-eclogite transformation. Journal of Petrology 7, 337–362.

Lachance, G.R., Trail, R.J., 1966. Practical solution to the matrix problem in X-ray analysis. Canadian Spectroscopy 11, 43–48.

Laubier, M., Grove, T.L., Langmuir, C.H., 2014. Trace element mineral/melt partitioning for basaltic and basaltic andesitic melts: an experimental and laser ICP-MS study with application to the oxidation state of mantle source regions. Earth and Planetary Science Letters 392, 265–278.

Leake, B.E., Woolley, A.R., Arps, C.E.S., Birch, W.D., Gilbert, M.C., Grice, J.D., Hawthorne, F.C., Kato, A., Kisch, H.J., Krivovichev, V.G., Linthout, K., Laird, J., Mandarino, J.A., Maresch, W.V., Nickel, E.H., Rock, N.M.S., Schumacher, J.C., Smith, D.C., Stephenson, N.C.N., Ungaretti, L., Whittaker, E.J.W., Youzhi, G., 1997. Nomenclature of amphiboles: report of the subcommittee on amphiboles of the international mineralogical association, commission on new minerals and mineral names. American Mineralogist 82, 1019–1037.

Lensch, G., Davoudzadeh, M., 1982. Ophiolites in Iran. Neues Jahrbuch für Geologie und Paläontologie 5, 306–320.

Liang, Y., Sun, C., Yao, L., 2013. A REE-two-pyroxene thermometer for mafic and ultramafic rocks. Geochimica et Cosmochimica Acta 102, 246–260.
Loocke, M., Snow, J.E., 2013. Melt stagnation in peridotites from the Godzilla Megamullion oceanic core complex, Parece Vela basin, Philippine Sea. Lithos 183, 1–10.
Lykins, R.W., Jenkins, D.M., 1992. Experimental determination of pargasite stability relations in the presence of orthopyroxene. Contributions to Mineralogy and Petrology 112, 405–413.
Mattei, M., Cifelli, F., Muttoni, G., Rashid, H., 2014. Post-Cimmerian (Jurassic–Cenozoic) paleogeography and vertical axis tectonic rotations of Central Iran and the Alborz Mountains. Journal of Asian Earth Sciences 102, 92–101.
McKay, G., 2004. The europium oxybarometer: power and pitfalls. Workshop on Oxygen in the Terrestrial Planets. 46, p. 3036.
Mehdipour Ghazi, J., Moazzen, M., Rahgoshay, M., Shafaii Moghadam, H., 2010. Mineral chemical composition and geodynamic significance of peridotites from Nain ophiolite, central Iran. Journal of Geodynamics 49, 261–270.
Menzies, M.A., Hawkesworth, C.J., 1987. Mantle Metasomatism. Academic Press (472 pp.).
Mercier, J.C.C., Nicolas, A., 1975. Textures and fabrics of upper-mantle peridotites as illustrated by xenoliths from basalts. Journal of Petrology 16, 454–487.
Miller, C., Zanetti, A., Thöni, M., Konzett, J., Klötzli, U., 2012. Mafic and silica-rich glasses in mantle xenoliths from Wau-en-Namus, Libya: textural and geochemical evidence for peridotite-melt reactions. Lithos 128-131, 11–26.
Möller, P., Muecke, G.K., 1984. Significance of europium anomalies in silicate melts and crystal-melt equilibria: a re-evaluation. Contributions to Mineralogy and Petrology 87, 242–250.
Montanini, A., Tribuzio, R., Anczkiewicz, R., 2006. Exhumation history of a garnet pyroxenite-bearing mantle section from a continent-ocean transition (Northern Apennine ophiolites, Italy). Journal of Petrology 47, 1943–1971.
Morishita, T., Ishida, Y., Arai, S., 2005a. Simultaneous determination of multiple trace element compositions in thin (b30 μm) layers of BCR-2G by 193 nm ArF excimer laser ablation-ICP-MS: implications for matrix effect and elemental fractionation on quantitative analysis. Geochemical Journal 39, 327–340.
Morishita, T., Ishida, Y., Arai, S., Shirasaka, M., 2005b. Determination of multiple trace element compositions in thin (b30 μm) layers of NIST SRM 614 and 616 using laser ablation inductively coupled plasma mass spectrometry. Geostandards and Geoanalytical Research 29, 107–122.
Müntener, O., Pettke, T., Desmours, L., Meier, M., Schaltegger, U., 2004. Refertilization of mantle peridotite in embryonic ocean basins: trace element and Nd-isotope evidence and implications for crust-mantle relationships. Earth and Planetary Science Letters 221, 293–308.
Nimis, P., Ulmer, P., 1998. Clinopyroxene geobarometry of magmatic rocks part 1: an expanded structural geobarometer for anhydrous and hydrous basic and ultrabasic systems. Contributions to Mineralogy and Petrology 133, 122–135.
Niu, Y., Hékinian, R., 1997. Basaltic liquids and harzburgitic residues in the Garrett transform: a case study at fast-spreading ridges. Earth and Planetary Science Letters 146, 243–258.
Ohara, Y., Stern, R.J., Ishii, T., Yurimoto, H., Yamazaki, T., 2002. Peridotites from the Mariana trough: first look at the mantle beneath an active back-arc basin. Contributions to Mineralogy and Petrology 143, 1–18.
Okamura, H., Arai, S., Kim, Y.U., 2006. Petrology of forearc peridotite from the Hahajima seamount, the Izu-Bonin arc, with special reference to chemical characteristics of chromian spinel. Mineralogical Magazine 70, 15–26.
Ottonello, G., Joron, J.L., Piccardo, G.B., 1984. Rare Earth and 3d transition element geochemistry of peridotitic rocks: II. Ligurian peridotites and associated basalts. Journal of Petrology 25, 373–393.
Ozawa, K., Takahashi, N., 1995. P-T history of a mantle diapir: the Horoman peridotite complex, Hokkaido, northern Japan. Contributions to Mineralogy and Petrology 120, 223–248.
Piccardo, G.B., Vissers, R.L.M., 2007. The pre-oceanic evolution of the Erro-Tobbio peridotite (Voltri Massif, Ligurian Alps, Italy). Journal of Geodynamics 43, 417–449.
Piccardo, G.B., Rampone, E., Vannucci, R., Shimizu, N., Ottolini, L., Bottazzi, P., 1993. Mantle processes in the sub-continental lithosphere: the case study of the rifted spl-herzolites from Zabargad (Red Sea). European Journal of Mineralogy 5, 1039–1056.
Piccardo, G.B., Müntener, O., Zanetti, A., Romairone, A., Bruzzone, S., Poggi, E., Spagnolo, G., 2004. The Lanzo South peridotite: melt-peridotite interaction in the mantle lithosphere of the Jurassic Ligurian Tethys. Ofioliti 29, 37–62.
Pirnia, T., Arai, S., Torabi, G., 2010. Post-deformational impregnation of depleted MORB in Nain lherzolite (Central Iran). Journal of Mineralogical and Petrological Sciences 105, 74–79.
Pirnia, T., Arai, S., Torabi, G., 2013. A better picture of the mantle section of the Nain ophiolite inferred from detrital chromian spinels. The Journal of Geology 121, 645–661.
Pirnia, T., Arai, S., Tamura, A., Ishimaru, S., Torabi, G., 2014. Sr enrichment in mantle pyroxenes as a result of plagioclase alteration in lherzolite. Lithos 196-197, 198–212.
Presnall, D.C., Gudfinnsson, G.H., Walter, M.J., 2002. Generation of mid-ocean ridge basalt at pressure from 1 to 7 GPa. Geochimica et Cosmochimica Acta 66, 2073–2090.
Rahmani, F., Noghreyan, M., Khalili, M., 2007. Geochemistry of sheeted dikes in the Nain ophiolite (Central Iran). Ofioliti 32, 119–129.
Rampone, E., Borghini, G., 2008. The melt intrusion/interaction history of the Erro-Tobbio peridotites (Ligurian Alps, Italy): insights on mantle processes at non-volcanic passive margins. European Journal of Mineralogy 20, 573–585.
Rampone, E., Piccardo, G.B., Vannucci, R., Botazzi, P., Ottolini, L., 1993. Subsolidus reactions monitored by trace element partitioning: the spinel-to plagioclase facies transition in mantle peridotites. Contributions to Mineralogy and Petrology 115, 1–17.
Rampone, E., Hofmann, A.W., Piccardo, G.B., Vannucci, R., Bottazzi, R., Ottolini, L., 1995. Petrology, mineral isotope geochemistry of the external Liguride peridotites (Northern Apennines, Italy). Journal of Petrology 36, 81–105.
Rampone, E., Piccardo, G.B., Vannucci, R., Bottazzi, P., 1997. Chemistry and origin of trapped melts in ophiolitic peridotites. Geochimica et Cosmochimica Acta 61, 4557–4569.
Rampone, E., Hofmann, A.W., Raczek, I., 1998. Isotopic contrasts within the Internal Liguride ophiolite (N. Italy): the lack of a genetic mantle-crust link. Earth and Planetary Science Letters 163, 175–189.
Rampone, E., Romairone, A., Abouchami, W., Piccardo, G.B., Hofmann, W., 2005. Chronology, petrology and isotope geochemistry of the Erro-Tobbio peridotites (Ligurian Alps, Italy): records of late Paleozoic lithospheric extension. Journal of Petrology 46, 799–827.
Rampone, E., Piccardo, G.B., Hofmann, A.W., 2008. Multi-stage melt-rock interaction in the Mt. Maggiore (Corsica, France) ophiolitic peridotites: microstructural and geochemical evidence. Contributions to Mineralogy and Petrology 156, 453–475.
Robertson, A.H.F., 2007. Overview of tectonic settings related to the rifting and opening of Mesozoic ocean basins in the Eastern Tethys: Oman, Himalayas and Eastern Mediterranean regions. In: Karner, G., Manatschal, G., Pinheiro, L. (Eds.), Imaging, Mapping and Modelling Continental Lithosphere Extension and Breakup. Geological Society of London Special Publication 282, pp. 325–389.
Saccani, E., 2015. A new method of discriminating different types of post-Archean ophiolitic basalts and their tectonic significance using Th-Nb and Ce-Dy-Yb systematics. Geoscience Frontiers 6, 481–501.
Saccani, E., Allahyari, K., Beccaluva, L., Bianchini, G., 2013. Geochemistry and petrology of the Kermanshah ophiolites (Iran): implication for the interaction between passive rifting, oceanic accretion, and plume-components in the Southern Neo-Tethys Ocean. Gondwana Research 24, 392–411.
Saccani, E., Dilek, Y., Marroni, M., Pandolfi, L., 2015. Continental margin ophiolites of Neotethys: remnants of Ancient Ocean-continent transition zone (OCTZ) lithosphere and their geochemistry, mantle sources and melt evolution patterns. Episodes 38, 230–249.
Saccani, E., Dilek, Y., Photiades, A., 2017. Time-progressive mantle-melt evolution and magma production in a Tethyan marginal sea: a case study of the Albanide-Hellenide ophiolites. Lithosphere 10, 35–53.
Schwandt, C.S., McKay, G.A., 1998. Rare earth element partition coefficient from enstatite/melt synthesis experiment. Geochimica et Cosmochimica Acta 62, 2845–2848.
Seyler, M., Bonatti, E., 1997. Regional-scale melt-rock interaction in lherzolitic mantle in the Romanche fracture zone (Atlantic Ocean). Earth and Planetary Science Letters 146, 273–287.
Shafaii Moghadam, H., Whitechurch, H., Rahgoshay, M., Monsef, I., 2009. Significance of Nain-Baft ophiolite belt (Iran): short-lived, transtensional Cretaceous back-arc oceanic basins over the Tethyan subduction zone. Comptes Rendus Geoscience 341, 1016–1028.
Shafaii Moghadam, H., Stern, R.J., Rahgoshay, M., 2010. The Dehshir ophiolite (Central Iran): geochemical constraints on the origin and evolution of the Inner Zagros ophiolite belt. Geological Society of America Bulletin 122, 1516–1547.
Shahabpour, J., 2005. Tectonic evolution of the orogenic belt in the region located between Kerman and Neyriz. Journal of Asian Earth Sciences 24, 405–417.
Sibson, R.H., 1977. Fault rocks and fault mechanisms. Journal of the Geological Society 133, 191–213.
Sisson, T.W., 1994. Hornblende-melt trace-element partitioning measured by ion microprobe. Chemical Geology 117, 331–344.
Suhr, G., Seck, H.S., Shimizu, N., Gunther, D., Jenner, G., 1998. Circulation of refractory melts in the lower most oceanic crust: evidence from a trace element study of dunite hosted clinopyroxenes in the Bay of Island Ophiolite. Contributions to Mineralogy and Petrology 122, 387–405.
Sun, C., Liang, Y., 2012. Distribution of REE between clinopyroxene and basaltic melt along a mantle adiabat: effects of major element composition, water, and temperature. Contributions to Mineralogy and Petrology 163, 807–823.
Sun, S.S., McDonough, W.F., 1989. Chemical and isotopic systematics of oceanic basalts: implications for mantle composition and processes. In: Saunders, A.D., Norry, M.J. (Eds.), Magmatism in the Ocean Basins. Geological Society, London, Special Publication vol. 42, pp. 313–345.
Sun, C.O., Willians, R.J., Sun, S.-S., 1974. Distribution coefficient of Eu and Sr for plagioclase-liquid and clinopyroxene-liquid equilibria in oceanic ridge basalt: an experimental study. Geochimica et Cosmochimica Acta 38, 1415–1433.
Sun, S.S., Nesbitt, R.W., Sharaskin, A.Y., 1979. Geochemical characteristics of mid-ocean ridge basalts. Earth and Planetary Science Letters 44, 119–138.
Susini, S., Wezel, F.C., 1999. Percolated mantle peridotites along the Romanche fracture zone (Equatorial Atlantic Ocean). Rendiconti Fisiche Accademia Lincei 10, 231–255.
Takahashi, E., Uto, K., Schilling, J.G., 1987. Primary magma compositions and Mg/Fe ratios of their mantle residues along Mid Atlantic Ridge 29°N to 73°N. Technical Report of Institute for Study of the Earth's Interior. A9. Okayama University, Series, pp. 1–14.
Tang, M., McDonough, W.F., Ash, R.D., 2017. Europium and strontium anomalies in the MORB source mantle. Geochimica et Cosmochimica Acta 197, 132–141.
Tartarotti, P., Susini, S., Nimis, P., Ottolini, L., 2002. Melt migration in the upper mantle along the Romanche Fracture Zone (Equatorial Atlantic). Lithos 63, 125–149.
Vannucci, R., Piccardo, G.B., Rivalenti, G., Zanetti, A., Rampone, E., Ottolini, L., Oberti, R., Mazzucchelli, M., Bottazzi, P., 1995. Origin of LREE-depleted amphiboles in the subcontinental mantle. Geochimica et Cosmochimica Acta 59, 1763–1771.
Weill, D.F., McKay, G.A., 1975. In: Merrill, R.B., Hubbard, N.J., Mendell, W.W., Williams, R.J. (Eds.), The Partitioning of Mg, Fe, Sr, Ce, Sm, Eu, and Yb in Lunar Igneous Systems and a Possible Origin of KREEP by Equilibrium Partial Melting. Proceedings of the 6th Lunar Science Conference vol. 1. Pergamon Press, New York, pp. 1143–1158.
Witt-Eickschen, G., Seck, H.A., 1991. Solubility of Ca and Al in orthopyroxene from spinel peridotite: an improved version of an empirical geothermometer. Contributions to Mineralogy and Petrology 106, 431–439.

Workman, R.K., Hart, S.R., 2005. Major and trace element composition of the depleted MORB mantle (DMM). Earth and Planetary Science Letters 231, 53–72.

Zanetti, A., Vannucci, R., Bottazzi, P., Oberti, R., Ottolini, L., 1996. Infiltration metasomatism at Lherz and monitored by systematic ion-microprobe investigations close to a hornblendite vein. Chemical Geology 134, 113–133.

Zanetti, A., Oberti, R., Piccardo, G.B., Vannucci, R., 2000. Light lithophile (Li, Be and B) volatile (H, F and Cl) and trace elements composition of mantle amphiboles from Zabargad peridotite: insight into the multistage subsolidus evolution of subcontinental mantle during Red Sea rifting. Goldschmidt. Journal of Conference Abstracts 5 (2), 1120.